

**The chromatin factors SET-26 and HCF-1 oppose the histone deacetylase HDA-1 in longevity and gene regulation in *C. elegans***

Felicity J. Emerson<sup>1</sup>, Caitlin Chiu<sup>1</sup>, Laura Y. Lin<sup>1</sup>, Christian G. Riedel<sup>2</sup>, Ming Zhu<sup>3</sup>, and Siu Sylvia Lee<sup>1\*</sup>

<sup>1</sup>Department of Molecular Biology and Genetics, Cornell University, Ithaca, New York, United States of America

<sup>2</sup>Department of Biosciences and Nutrition, Karolinska Institutet, Huddinge, Sweden

<sup>3</sup>National Institute of Biological Sciences, Beijing, China

\*Corresponding author

Email: [sylvia.lee@cornell.edu](mailto:sylvia.lee@cornell.edu) (SSL)

## Abstract

SET-26, HCF-1, and HDA-1 are highly conserved chromatin factors with key roles in development and aging. Here we present mechanistic insights into how these factors regulate gene expression and modulate longevity in *C. elegans*. We show that SET-26 and HCF-1 cooperate to regulate a common set of genes, and both antagonize the histone deacetylase HDA-1 to limit longevity. We propose a model in which SET-26 recruits HCF-1 to chromatin in somatic cells, where they stabilize each other at the promoters of a subset of genes, particularly mitochondrial function genes, and regulate their expression. HDA-1 opposes SET-26 and HCF-1 on the regulation of a subset of their common target genes and in longevity. Our findings suggest that SET-26, HCF-1, and HDA-1 comprise a mechanism to fine-tune gene expression and longevity and likely have important implications for the mechanistic understanding of how these factors function in diverse organisms, particularly in aging biology.

## Introduction

Chromatin factors provide a layer of regulatory information for the genome by influencing the surrounding chromatin environment. They impact gene expression by modulating histone marks, DNA methylation, accessibility of chromatin, and the composition of protein complexes at chromatin. As such, chromatin factors have an essential role in biology and have been implicated in diverse biological processes from cell division<sup>1</sup> to aging<sup>2</sup>. Of particular interest, chromatin and aging are intricately linked. Many studies show correlations between aging and an altered chromatin environment (see<sup>3</sup> for review), but causative studies are challenging in humans and mammalian model organisms, which often have a relatively long natural lifespan. One of the best systems with which to study this relationship is the worm *C. elegans*, which shares many critical chromatin regulators with mammals<sup>4</sup> and is a robust model for aging due to its short lifespan and well-characterized aging pathways.

In *C. elegans*, manipulation of specific histone readers, writers, erasers, adaptors, and chromatin remodelers has been shown to influence longevity<sup>5–14</sup>, supporting a causative link between chromatin and aging. Chromatin factors that influence longevity have been demonstrated to work through many well-studied longevity pathways, including induction of the mitochondrial unfolded protein response (mitoUPR)<sup>9,11,13,14</sup>, lipid metabolism<sup>12</sup>, and insulin signaling<sup>6,7,10</sup>. Understanding the precise mechanism by which chromatin factors act to modulate aging will help us better understand the aging process itself and may guide efforts to improve healthy aging.

SET-26 and HCF-1 are two highly conserved chromatin factors that our lab has studied that influence longevity in *C. elegans*. SET-26, the *C. elegans* homolog of MLL5, is an epigenetic reader that binds to H3K4me3, a mark typically associated with active chromatin, via its PHD domain<sup>15</sup>. HCF-1, the *C. elegans* homolog of HCF-1, is a chromatin adaptor protein, well characterized in mammalian cells for recruiting histone modifying complexes to chromatin<sup>16</sup>. Loss of either SET-26 or HCF-1 leads to a long lifespan and increased stress resistance<sup>5,8,15,17</sup>. Evidence indicates that SET-26 and HCF-1 operate within somatic cells to limit lifespan<sup>5,15</sup>, and they function within the germline to regulate germline development and fertility<sup>15,18</sup>. Both SET-26 and HCF-1 require DAF-16 to modulate lifespan<sup>5,8,15,17</sup>, and HCF-1 also interacts with SIR-2.1 to affect lifespan<sup>17</sup>. Whereas SET-26 and HCF-1 share many similarities in how they impact longevity, their working relationship was not previously investigated.

Chromatin factors lacking enzymatic activity themselves, like SET-26 and HCF-1, often partner with additional enzymatic components that directly alter the chromatin environment<sup>16</sup>. Histone deacetylases are a major group of enzymes that remove histone acetylation, a mark typically associated with active chromatin<sup>19</sup>. The histone deacetylase HDA-1, the *C. elegans* homolog of HDAC1 and HDAC2, is a critical regulator of development, neurodegeneration, and the mitoUPR<sup>13,14,20,21</sup>, a stress response program that communicates mitochondrial stress to the nucleus and initiates transcriptional activation of mitochondrial chaperones and proteases<sup>22</sup>.

HDA-1 is required for the long lifespan of a model of mitoUPR activation<sup>13</sup>, but its role in the lifespan of other longevity models has not yet been explored.

Here we show that SET-26 and HCF-1 are functional partners in longevity and chromatin regulation in *C. elegans*. We find that SET-26 and HCF-1 operate in the same genetic pathway to regulate lifespan, they share many common binding sites at chromatin, and they influence somatic gene expression in similar ways. Our data suggest that SET-26 plays a major role in recruiting HCF-1 to chromatin in *C. elegans* somatic cells, where, at a subset of binding sites, HCF-1 plays a minor role in stabilizing SET-26 binding as well. We find that the long lifespan of both the *set-26(-)* and *hcf-1(-)* mutants depends on HDA-1, and we posit that all three factors co-regulate a common set of genes, likely those involved in mitochondrial metabolism, with HDA-1 antagonizing SET-26 and HCF-1 for control over gene expression.

## Results

### SET-26 and HCF-1 work together to modulate lifespan

Previous work has demonstrated that loss of either SET-26<sup>8,15</sup> or HCF-1<sup>5,17</sup> leads to a longer lifespan in *C. elegans*, however the mechanism of lifespan extension for either of these mutants is incompletely understood, and functional cooperative partners for these proteins have not been identified. Previous analysis of HCF-1 binding partners in *C. elegans* through immunoprecipitation mass spectrometry (IP-Mass spec)<sup>17</sup> identified SET-26 as a high confidence interactor, suggesting the two proteins could be part of the same complex. Consistent with our IP-Mass spec observation, MLL5 and HCF-1, the human homologs of SET-26 and HCF-1, are able to physically interact and form a complex via an “HCF1 binding motif” present in the MLL5 protein<sup>23</sup>, which is well conserved from worms to humans (Supplementary Fig. 1a). We reasoned that if SET-26 and HCF-1 are functional partners, they should operate in the same genetic pathway to modulate longevity. We tested the *set-26(tm2467) hcf-1(pk924)* double

mutant and observed that loss of *set-26* did not significantly further extend the long lifespan of the *hcf-1(-)* mutant (Fig. 1a). This non-additive effect is consistent with the hypothesis that the two genes operate in the same genetic pathway to modulate lifespan.

### **SET-26 and HCF-1 bind common gene targets**

Next, we wondered whether SET-26 and HCF-1 occupy similar binding sites at chromatin, as would be expected if they are part of the same protein complex. To test this, we first constructed CRISPR knock-in strains containing tagged SET-26 or HCF-1. Notably, the tagged strains for both SET-26 and HCF-1 had normal lifespans (Supplementary Fig. 1b, c), indicating that the tags did not disrupt the normal protein function.

We then performed the chromatin profiling technique, CUT&RUN (Cleavage under targets and release using nuclease) with tagged SET-26 or HCF-1. Since our previous work indicated that SET-26 and HCF-1 act in somatic cells to modulate lifespan<sup>5,15</sup>, we specifically profiled SET-26 and HCF-1 genomic binding in somatic cells using a germline-less mutant background. This approach was especially critical because SET-26 and HCF-1 both have separate functions in the germline to regulate development and reproduction<sup>15,18</sup>, and due to the large size of the *C. elegans* germline<sup>24</sup>, utilizing only wildtype worms would risk diluting any somatic-specific signal that could be the most relevant for longevity. The CUT&RUN data indicated that the biological replicates were well correlated with each other (Supplementary Fig. 1d), indicating the results were highly reproducible. As previously shown, the SET-26 binding profile obtained by CUT&RUN was highly similar to the previous ChIP-seq profile for SET-26 obtained from our lab<sup>15,25</sup>. SET-26 and HCF-1 binding were both enriched in promoter regions in the *C. elegans* genome (Supplementary Fig. 1e, f), with high enrichment immediately upstream of the transcription start site (TSS) (Fig. 1b, c). This is consistent with previous ChIP-seq data of HCF-1 from mammalian cells<sup>26,27</sup>, as well as our lab's previous SET-26 ChIP-seq data in *C.*

*elegans*, which indicated that SET-26 is an H3K4me3 reader and binds to many active promoters containing H3K4me3<sup>15</sup>.

The somatic binding profiles of SET-26 and HCF-1 were highly similar (Fig. 1d-f), with 76% of HCF-1 peaks overlapping with SET-26 peaks and 55% of SET-26 peaks overlapping with HCF-1 peaks. Moreover, we found that within these common peak regions, SET-26 and HCF-1 binding were centered directly on top of each other (Fig. 1g). We next associated SET-26 and HCF-1 peaks to their closest promoters<sup>28</sup> to identify the putative target genes regulated by SET-26 and HCF-1. As expected, the majority of their putative target genes were shared (Fig. 1h). Functional enrichment analysis indicated that the SET-26 and HCF-1 commonly-bound genes were enriched for many biological processes, with the most highly significant being mitochondrial metabolism, mRNA processing, and ribosome subunits (Fig. 1i). Taken together, these results suggest that SET-26 and HCF-1 both bind to the promoters of many genes important for basic biological functions in worms.

To confirm that the main findings from this analysis also extended to wild-type worms, we performed the same CUT&RUN analysis in the wildtype background and obtained similar results (Supplementary Fig. 1g-j). Interestingly, while the majority of genes bound by SET-26 and HCF-1 were identified in both wildtype and somatic-specific analysis (Supplementary Fig. 1k-l), the genes identified as bound by SET-26 and HCF-1 only in wildtype worms containing germlines were enriched for additional functional groups, including cell cycle (Supplementary Fig. 1m-n), consistent with important roles for SET-26 and HCF-1 in the cell cycle as has been demonstrated in mammalian cells<sup>16,23</sup>.

### **SET-26 and HCF-1 regulate expression of a common set of genes**

To better understand how SET-26 and HCF-1 regulate the genes to which they bind, we performed RNA-seq of germline-less *set-26(-)* and *hcf-1(-)* mutants at the same time point as our CUT&RUN experiments (day 1 adulthood) (Supplementary Fig. 2a). Differential expression

analysis revealed highly overlapping RNA expression changes in *set-26(-)* and *hcf-1(-)* mutants (Fig. 2a-c), suggesting similar pathways are activated and repressed in both longevity mutants. Pathway enrichment analysis indicates that the 485 genes commonly upregulated in germline-less *set-26(-)* and *hcf-1(-)* mutants are most enriched for mitochondrial metabolism, and collagen/extracellular matrix (Supplementary Fig. 2b), while the 602 commonly downregulated genes are most significantly enriched for pathogen stress response and lipid metabolism (Supplementary Fig. 2c).

We focused on the putative direct targets of SET-26 and HCF-1 that are likely to have biological relevance under our assaying condition, which are the genes bound by each of the factors that also showed expression changes when each of the factors was lost. Notably, similar numbers of SET-26 and HCF-1 direct targets showed up- or downregulated mRNA expression in the mutants (Fig. 2d), suggesting that SET-26 and HCF-1 could have both activating and repressive roles depending on the gene. The SET-26 and HCF-1 targets commonly upregulated in *set-26(-)* and *hcf-1(-)* mutants were enriched for mitochondrial metabolism, ribosome biogenesis, and mRNA binding (Fig. 2e), whereas the downregulated common targets were enriched for lipid metabolism, short chain dehydrogenase metabolism, and pathogen stress response (Fig. 2f), suggesting SET-26 and HCF-1 could have direct roles in regulating these pathways.

### **SET-26 is required for HCF-1's recruitment to chromatin at the majority of HCF-1 binding sites**

We next wondered what relationship SET-26 and HCF-1 have with each other at chromatin. SET-26 and its' mammalian homolog, MLL5, have both been previously described to bind to the active H3K4me3 histone mark<sup>15,29</sup>, which could account for their method of recruitment to chromatin. HCF-1 however, does not possess any DNA or chromatin binding domains itself, and the mammalian homolog is often recruited by other chromatin factors,

including MLL5<sup>16,30</sup>, to large protein complexes. To determine whether SET-26 could recruit HCF-1 to chromatin in somatic cells of *C. elegans*, we obtained the chromatin binding profile of HCF-1 using our HCF-1-tagged strain in germline-less worms with and without functional *set-26*. In order to appropriately compare HCF-1 binding profiles between genotypes, we additionally surveyed H3 binding in each genotype in parallel and normalized HCF-1 binding to H3 within each genotype. We found that normalizing to antibody background as in Fig. 1 or to H3 made little difference in the appearance of the HCF-1 profile or the location of peaks called by MACS2 (Supplementary Fig. 3a), and the H3 profiles were highly consistent between controls and *set-26(-)* mutants (Supplementary Fig. 3b). We therefore used H3 as normalization for further differential analysis.

A survey of the HCF-1 peak regions revealed a consistent and dramatic decrease in HCF-1 binding in somatic cells of the *set-26(-)* mutant (Fig. 3a), such that the number of HCF-1 somatic peaks was reduced by 88% in the *set-26(-)* background (Fig. 3b). To visualize this genome-wide, we plotted HCF-1 binding at all HCF-1 somatic peak regions and noticed a drastic decrease in binding in the *set-26(-)* mutant at most HCF-1 peaks (Fig. 3c). While there is still some enrichment of HCF-1 at binding sites in the *set-26(-)* mutant above background levels, we conclude that SET-26 is required for the majority of proper HCF-1 patterning at chromatin genome-wide in somatic cells. *hcf-1* RNA and protein levels are not noticeably changed in the germline-less *set-26(-)* mutant (Supplementary Fig. 3c-e), suggesting that the decrease of HCF-1 binding to chromatin is not due to a defect in HCF-1 production in *set-26(-)* mutants.

We next asked which HCF-1 somatic binding regions were statistically significantly decreased in the *set-26(-)* mutant compared to controls, and we observed that 82% of HCF-1 peaks exhibited significantly lower binding in the *set-26(-)* mutant (Fig. 3d), with a substantial average fold change decrease (0.16). We next asked which of these *set-26*-dependent HCF-1-bound regions were associated with genes that showed significant RNA expression change in somatic cells of *set-26(-)* and *hcf-1(-)* mutants (Fig. 3e). We found that the expression of 319 of

the *set-26*-dependent HCF-1-bound genes showed significant RNA expression change, with similar numbers of up- and downregulated genes. The upregulated genes were strongly enriched for mitochondrial metabolism, with less significant enrichment for ribosome biogenesis and mRNA binding (Fig. 3f), while the downregulated genes were enriched for lipid and mitochondrial metabolism (Fig. 3g). The data suggest that SET-26 could play a critical role in either recruiting or stabilizing HCF-1 binding at chromatin, where the two factors work together to fine-tune gene expression, particularly of mitochondrial and lipid metabolism genes. To confirm that the dramatic germline-less results we obtained were not due to the RNAi system used to produce germline-less worms (*glp-1* RNAi), we repeated the experiments with a genetic perturbation to produce germline-less worms (*glp-1(e2141)*) and obtained similar results (Supplementary Fig. 3f-g), with 80% of peaks being significantly decreased by loss of *set-26* (Supplementary Fig. 3h).

When we repeated these experiments in whole worms containing germlines, we observed a moderate loss of HCF-1 recruitment to chromatin in the *set-26(-)* mutant worms (Supplementary Fig. 3i-j), with only 9% of HCF-1 peaks being significantly lowered in worms lacking *set-26* (Supplementary Fig. 3k). As SET-26 primarily operates in somatic cells to modulate lifespan<sup>15</sup>, we focused on the somatic results, which we believe to be the most relevant to potentially help us understand the lifespan phenotypes of the mutants.

### **HCF-1 is dispensable for most SET-26 recruitment, but does contribute to SET-26 stabilization at a subset of genes**

We next tested the opposite hypothesis, examining whether SET-26 recruitment to chromatin also required HCF-1. We performed CUT&RUN targeting SET-26 in germline-less worms with and without functional *hcf-1* (Suppl Fig. 4a), and we did not observe a dramatic difference in SET-26 recruitment to chromatin (Fig. 4a-c). We wondered whether individual SET-26 peak regions at local sites may still reach the threshold for being significantly changed

in the *hcf-1* mutant. We identified 37% of SET-26 somatic peaks were significantly decreased by loss of *hcf-1* (Fig. 4d), with a modest average fold change decrease (0.51). These binding differences were largely unique to somatic cells as well, as, when we repeated the experiments in whole worms containing germlines, only 2% of SET-26 binding regions were identified as significantly altered in *hcf-1(-)* mutants (Supplementary Fig. 4b-d). We asked which of the *hcf-1*-dependent SET-26-bound regions identified in somatic cells were associated with genes that showed significant RNA expression change in somatic cells of *set-26(-)* and *hcf-1(-)* mutants (Fig. 4e). 238 *hcf-1*-dependent SET-26-bound genes showed significant expression changes in the somatic *set-26(-)* and *hcf-1(-)* mutants, again with a similar number of up- and down-regulated genes. The upregulated genes were enriched for mitochondrial metabolism, ribosome biogenesis, and mRNA binding (Fig. 4f), while the downregulated genes were enriched for lipid metabolism (Fig. 4g).

Since these genes represent similar biological categories to the genes identified in Figure 3e-g as having decreased HCF-1 binding in the *set-26(-)* germline-less mutant and exhibiting expression changes in the mutants, we asked how many of the genes from the two analyses overlapped. We found that the majority of the genes did overlap (Fig. 4h, i), with 122 upregulated and 79 downregulated genes in common. As expected, the 122 upregulated genes were enriched for mitochondrial metabolism, ribosome biogenesis, and mRNA binding (Supplementary Fig. 4e) while the 79 downregulated genes were enriched for lipid metabolism (Supplementary Fig. 4f). Overall, the data suggest that SET-26 and HCF-1 could co-stabilize each other on a subset of direct target genes involved in key biological processes.

### **HDA-1 is required for the full longevity of *set-26(-)* and *hcf-1(-)* mutants**

Because SET-26 and HCF-1 homologs are well known to work in large complexes of chromatin factors<sup>23,26,30,31</sup>, we wondered whether we could identify additional protein factors that might work together with SET-26 and HCF-1 at chromatin in *C. elegans*. We returned to the IP-

Mass Spec for *C. elegans* HCF-1 interactors and were particularly interested to find the histone deacetylase HDA-1, homolog of mammalian HDAC1 and HDAC2. Homologs of SET-26 and HCF-1 in flies and humans, respectively, have been described to recruit HDAC1 homologs to chromatin<sup>16,32</sup>, supporting a conserved role for an interaction between these three proteins in various species.

We next tested whether *hda-1* depletion would impact the lifespan of our *set-26(-)* and *hcf-1(-)* mutants. Previous studies have found that, depending on conditions, depletion of *hda-1* can either reduce<sup>13</sup>, or have no effect<sup>33,34</sup> on lifespan in *C. elegans*. However, the standard method of initiating *hda-1* RNAi at egg lay in *C. elegans* leads to a profound sterility and developmental phenotype, resulting in worms with a sterile and disorganized gonad and protruding vulva<sup>21</sup>. To avoid these pleiotropic developmental effects and to focus on the effect of *hda-1* depletion during aging, we initiated *hda-1* RNAi on day 1 of adulthood in all our studies. We found that under these conditions, depletion of *hda-1* with two different RNAi constructs (Supplementary Fig. 5a, b) did not impact the lifespan of wildtype worms, as previously reported for RNAi initiated at the L4 stage<sup>33</sup>. Interestingly, depletion of *hda-1* in adulthood specifically decreased the lifespan of *set-26(-)* and *hcf-1(-)* mutants (Fig. 5a and Supplementary Fig. 5c). Repeating this experiment in a germline-less mutant background, we obtained similar results (Fig. 5b), suggesting that HDA-1 is required in somatic cells of *set-26(-)* and *hcf-1(-)* mutants, where SET-26 and HCF-1 operate to modulate longevity.

### **HDA-1 co-occupies promoters bound by SET-26 and HCF-1**

Although histone deacetylases are typically associated with gene silencing by removing active acetylation marks, the mammalian HDAC1 has been shown to localize at active gene promoters<sup>19,35</sup>. Recent ChIP-seq data in *C. elegans* from germline-less mutants also supports the localization of HDA-1 to active promoters in the worm<sup>13</sup>. To repeat this observation in our own hands, we tagged HDA-1 with GFP and HA. We performed CUT&RUN with this HDA-1-

tagged strain in germline-less mutants (Supplementary Fig. 5d) and noticed that HDA-1 peaks were often (81% of the time) overlapping with promoter regions (Supplementary Fig. 5e), and, like SET-26 and HCF-1, the HDA-1 signal was enriched preceding the TSS (Fig. 5c). HDA-1 co-occupied many of the same promoters as SET-26 and HCF-1 (Fig. 5d-f), with 54% of HDA-1 peaks overlapping both SET-26 and HCF-1 somatic peaks, 49% of SET-26 peaks overlapping both HCF-1 and HDA-1 peaks, and 70% of HCF-1 peaks overlapping both SET-26 and HDA-1 peaks. This suggests that all three factors could regulate a common set of genes. Similar results were obtained by repeating the experiment in whole worms containing a germline (Supplementary Fig. 5f-i).

### **HDA-1 binding to chromatin is not detectably changed in *set-26(-)* or *hcf-1(-)* mutants**

We next wondered whether HDA-1 localization to chromatin was dependent on SET-26 or HCF-1. We performed CUT&RUN using germline-less HDA-1-tagged worms in *set-26(-)* and *hcf-1(-)* mutants (Supplementary Fig. 6a). We did not detect major differences in HDA-1 recruitment in *set-26(-)* or *hcf-1(-)* germline-less mutants (Fig. 6a-c), although the overall somatic HDA-1 signal and number of peaks was somewhat lower particularly in *set-26(-)* mutants. This was accompanied by the identification of 26% of HDA-1 somatic peaks as being significantly lower in the *set-26(-)* mutant (Fig. 6d), while only 5% of peaks were lower in the *hcf-1(-)* mutant (Fig. 6e). When we repeated the experiment in whole worms containing a germline (Supplementary Fig. 6b-c), the effect of *set-26* loss on HDA-1 recruitment to chromatin was more dramatic, with 64% of HDA-1 peaks showing decreased binding (Supplementary Fig. 6d), whereas loss of *hcf-1* continued to have a minimal effect on HDA-1 recruitment to chromatin (Supplementary Fig. 6e). Our data suggest that SET-26 works primarily in the germline to affect HDA-1 recruitment, and is unlikely to be related to the longevity phenotype of the *set-26(-)* mutant. This notion is further supported by the observation that only a small number of genes with lower somatic HDA-1 binding in *set-26(-)* and *hcf-1(-)* mutants also showed gene

expression changes in those mutants (Fig. 6f). Altogether, we suggest that altering HDA-1 recruitment in early adulthood is not the main mechanism through which *set-26(-)* and *hcf-1(-)* mutants extend lifespan.

### **HDA-1 regulates expression of a subset of SET-26 and HCF-1 targets in opposing directions in the soma of *set-26(-)* and *hcf-1(-)* mutants**

We next wondered whether the interaction between SET-26, HCF-1, and HDA-1 could be at the level of gene regulation. Given the antagonistic relationship between HDA-1 with SET-26 and HCF-1 in terms of lifespan modulation, we hypothesized that HDA-1 would oppose SET-26 and HCF-1 in gene regulation. We performed RNA-seq of germline-less *set-26(-)* and *hcf-1(-)* mutants and controls aged on either *hda-1* RNAi or empty vector control to determine *hda-1*-dependent gene expression changes. We collected samples at day 3, roughly 48 hours after initiating *hda-1* RNAi, and at day 12 of adulthood to examine any age-related changes. Surprisingly, we found that, although protein levels of HDA-1 were decreased after two days of *hda-1* RNAi (Supplementary Fig. 7a-b), gene expression was largely unchanged (Supplementary Fig. 7c). By day 12 of adulthood however, *hda-1*-dependent gene expression changes emerged (Supplementary Fig. 7d), and we therefore focused our analysis on these later-life gene expression changes.

We first looked for *hda-1*-dependent gene expression changes unique to *set-26(-)* and *hcf-1(-)* mutants, reasoning that since *hda-1* RNAi shortens the lifespan of *set-26(-)* and *hcf-1(-)* mutants and not controls, the *hda-1*-dependent gene expression changes unique to *set-26(-)* and *hcf-1(-)* mutants would be the best candidates for those responsible for the lifespan interaction. We plotted the expression of these genes first at baseline, in *set-26(-)* or *hcf-1(-)* day 12 mutants compared to controls, and then in *set-26(-)* and *hcf-1(-)* mutants on *hda-1* RNAi compared to empty vector (Fig. 7a). We split the heatmap into three segments based on different patterns of gene expression behavior, and were particularly interested in cluster 1 and

cluster 3, which generally showed opposing expression changes in *set-26(-)* and *hcf-1(-)* mutants on control vs *hda-1* RNAi. These are the best candidates for longevity genes dependent on *hda-1*, as they are genes that normally change in expression in one direction in long-lived *set-26(-)* and *hcf-1(-)* mutants, then change in the opposite direction in shorter lived *set-26(-)* and *hcf-1(-)* mutants on *hda-1* RNAi. We found that Cluster 1, which contained genes that tended to increase in *set-26(-)* and *hcf-1(-)* mutants but decreased on *hda-1* RNAi, was enriched for lipid and mitochondrial metabolism genes among others (Fig. 7b), while Cluster 3, which contained genes that tended to decrease in *set-26(-)* and *hcf-1(-)* mutants but increased on *hda-1* RNAi, was enriched for unassigned processes and collagen (Fig. 7c).

We were particularly interested in the enrichment in Cluster 1 for mitochondrial metabolism genes, given our findings that SET-26 and HCF-1 stabilize each others' binding on mitochondrial metabolism genes and the expression of these genes are increased in *set-26(-)* and *hcf-1(-)* mutants (Fig. 4h, Supplementary Fig. 4e). Furthermore, previous studies have demonstrated that HDA-1 is required for activation of the mitoUPR in *C. elegans*<sup>13,14</sup>, and the lifespan phenotype of a model of mitoUPR-mediated longevity<sup>13</sup>. Our RNA-seq analysis showed elevated levels of two mitoUPR markers, *hsp-6* and *hsp-60*<sup>36</sup>, in *set-26(-)* and *hcf-1(-)* young adults (Supplementary Fig. 7e,f), suggesting the mitoUPR is activated at baseline in these mutants. Previous analysis from Shao et al. identified a group of "HDA-1-dependent mitoUPR genes", which are mitoUPR genes normally activated upon mitochondrial perturbation and the expression of which decreases on *hda-1* RNAi<sup>13</sup>. We intersected this gene list with our CUT&RUN datasets to obtain "HDA-1-dependent mitoUPR genes" also bound by SET-26, HCF-1, and HDA-1 in somatic cells. We plotted the expression of these genes (Fig. 7d) in our day 12 adult gene expression data set and found that they tended to increase in expression in germline-less *set-26(-)* and *hcf-1(-)* mutants compared to controls, but that, when exposed to *hda-1* RNAi, the expression of these genes generally decreased in both *set-26(-)* and *hcf-1(-)* mutants. This is consistent with reduction of *hda-1* leading to a mild deactivation of mitoUPR

genes in germline-less *set-26(-)* and *hcf-1(-)* mutants. Interestingly, we found that many of these direct targets that were “HDA-1-dependent mitoUPR genes” were the same genes identified in Fig. 4h that exhibited de-stabilized SET-26 and HCF-1 binding in the *hcf-1(-)* and *set-26(-)* mutants respectively and were accompanied by increased RNA expression in both mutants at day 1 of adulthood (Fig. 7e). Taken together, this suggests that SET-26 and HCF-1 stabilize each other and dampen expression of a subset of mitoUPR genes where they compete with HDA-1 for control over gene expression.

## Discussion

In this study, we find that the chromatin factors SET-26 and HCF-1 work together in both lifespan modulation and chromatin regulation in *C. elegans*. We show that SET-26 and HCF-1 operate in the same genetic pathway to regulate lifespan, and the long lifespan of both mutants requires the histone deacetylase HDA-1 in somatic cells. All three factors have similar binding profiles at chromatin, suggesting they could regulate similar genes. Our CUT&RUN data suggests a more direct relationship between SET-26 and HCF-1 at chromatin, and we propose that SET-26 is responsible for the majority of HCF-1 recruitment to chromatin in somatic cells. Interestingly, we identified a subset of genes, mainly functioning in mitochondrial metabolism, on which SET-26 and HCF-1 stabilize each others' binding and act to affect the expression. The genetic relationship between HDA-1 with SET-26 and HCF-1 is antagonistic and our gene expression profiling shows that HDA-1 often impacts gene expression in the opposite direction from SET-26 and HCF-1, especially on mitochondrial metabolism genes. Taken together, we put forth a model in which SET-26 recruits HCF-1 to chromatin, where HCF-1 helps stabilize SET-26 at a subset of binding sites. HDA-1 binds to these same genes and antagonizes SET-26 and HCF-1 over control of gene expression (Fig. 7f). Together, SET-26, HCF-1, and HDA-1 fine-tune gene expression, particularly of mitochondrial metabolism genes.

Since previous studies have shown that both SET-26 and HCF-1 operate in somatic cells to regulate lifespan<sup>5,15</sup>, we focused the majority of our genomic studies on germline-less mutants to study the tissues of most relevance to the aging phenotype. Indeed, we found that HCF-1 binding to chromatin is severely affected by loss of *set-26* when looking at somatic-only samples but only minorly affected in whole worm samples, leading us to conclude that SET-26 could play a major role in recruiting HCF-1 to chromatin in somatic cells, rather than in the germline. This could be the result of a tissue specific role for SET-26 in recruiting HCF-1 only in somatic cells, or it could suggest that another protein contributes to HCF-1 recruitment in the germline. SET-9, a paralog of SET-26 which is only expressed in the germline and modulates reproduction but not lifespan<sup>15</sup>, would be the best candidate to fulfill this role, and it will be interesting for future studies to investigate whether SET-9 plays a role in recruiting HCF-1 in the germline. As *C. elegans* somatic cells are all terminally differentiated, this study may also provide incentive to study the role of the human homologs of SET-26 and HCF-1, called MLL5 and HCF-1, in differentiated cells. Most research on MLL5 and HCF-1 has been done in proliferating cell lines to study cell cycle progression and cancer, but recent evidence suggests both MLL5 and HCF-1 can play a role in neuronal development<sup>37,38</sup>, and HCF-1 has been shown to play a role in the adult murine liver<sup>27</sup>, highlighting the need for additional work on the mammalian homologs in differentiated tissues.

Contrarily, we find that HDA-1 binding to chromatin is more affected by loss of *set-26* in whole worm samples than in somatic-only samples, suggesting a possible role for germline SET-26 in mediating HDA-1 recruitment. In light of our previous observation that SET-9 and SET-26 are required to restrict spreading of H3K4me3 at SET-9 and SET-26 binding sites only in the germline<sup>15</sup>, it will be interesting to investigate whether histone acetylation and HDA-1 recruitment are also altered specifically at these sites. Given that SET-26, HCF-1, and HDA-1 are all well-known regulators of the germline in *C. elegans*<sup>15,18,21</sup> and that in *Drosophila* the SET-26 homolog, UpSET, can recruit the HDA-1 homolog, Rpd3, to chromatin in an embryonic cell

line<sup>32</sup>, this will be an interesting avenue for future study. It may prove especially interesting given the role of all three proteins in the cell cycle and cancer in humans<sup>16,39–41</sup>, and the evidence from our whole worm CUT&RUN data that SET-26 and HCF-1 binding is enriched for cell cycle genes in the germline.

In order to focus on the targets most likely to influence longevity, we characterized SET-26 and HCF-1 binding primarily in somatic cells. Interestingly, SET-26 and HCF-1 both occupy the promoters of many thousands of genes which represent a wide range of basic biological functions, making them relatively ubiquitous and general factors at promoters. However, only a small subset of these binding sites actually change in expression in *set-26(-)* and *hcf-1(-)* germline-less mutants. Previous studies of HCF-1 in mammalian cells have shown similar findings, revealing HCF-1 to be a factor that binds thousands of active promoters, but influences the expression of only a subset of those promoters in both activating and repressive ways<sup>26,27</sup>. Interestingly, mammalian HCF-1 is well known to be able to recruit either activating or repressive histone modifying complexes to chromatin at different stages of the cell cycle<sup>16</sup>. Thus, it is possible that SET-26 and HCF-1 interact with multiple chromatin modifying complexes or transcription factors in the same cell type, or, given that the CUT&RUN and RNA-seq data both represent a mixture of somatic cells, that SET-26 and HCF-1 work with distinct subcomplexes in different cell types. It will be interesting to identify these potential subcomplexes in the future, the cell type they operate in, and which contribute to the longevity phenotype of the mutants. It will also be interesting to determine whether the genes bound by SET-26 and HCF-1 that do not change in expression in our dataset ever show expression changes in different cell types or physiological contexts, and if not, whether SET-26 and HCF-1 are functionally redundant at those sites or if they play a different role in shaping the chromatin landscape.

One of the most interesting findings from this paper is that in somatic cells, HCF-1 binding is severely decreased genome-wide upon loss of *set-26*, whereas the majority of

somatic SET-26 binding occurs largely independently from HCF-1. While we have not completely ruled out an indirect effect caused by loss of *set-26*, it is tempting to speculate that SET-26 may directly recruit HCF-1 to chromatin. This is especially intriguing given evidence from human cells that mammalian homologs, MLL5 and HCF-1, directly interact<sup>23,30</sup>, and recent work that showed MLL5 was required for proper HCF-1 recruitment at certain MLL5 target genes<sup>30</sup>. It will be interesting in the future to determine whether the highly conserved “HCF-1 binding motif” identified in the human MLL5 protein<sup>23</sup> is also required for the interaction between *C. elegans* SET-26 and HCF-1. We posit that SET-26 arrives at chromatin first, recruited to H3K4me3 by its PHD domain<sup>15</sup>, and then serves as a major recruiter of HCF-1. This also may explain both the longevity of the *set-26(-)* mutant, caused by a lack of complete HCF-1 binding to chromatin, and the reason why the *set-26(-)* mutant is less long-lived than that *hcf-1(-)* mutant, as even the HCF-1 peaks that show a dramatic reduction in the *set-26(-)* mutant often still have some low level of HCF-1 present.

Although the majority of SET-26 recruitment is not altered by loss of *hcf-1*, there were still a subset of binding sites with decreased SET-26 binding in the *hcf-1(-)* mutant, suggesting that HCF-1 could help stabilize SET-26 at chromatin after being recruited. Interestingly, we found a subset of genes which exhibited lower SET-26 binding in the *hcf-1(-)* mutant, lower HCF-1 binding in the *set-26(-)* mutant, and altered RNA expression in both mutants. The upregulated genes were most enriched for mitochondrial metabolism, while the downregulated genes were enriched for lipid metabolism, implicating SET-26 and HCF-1 together as important direct co-regulators of these pathways.

In line with a conserved role for SET-26 and HCF-1 in modulating mitochondrial gene expression, evidence from mammals also finds that reduction in HCF-1 binding at chromatin in human cells impacts mitochondrial pathways<sup>31</sup> and loss of MLL5 in murine cells leads to increased mitochondrial membrane potential and ROS levels<sup>42</sup>. In an analysis similar to that shown here, wherein Minocha et al. overlapped their ChIP-seq and RNA-seq data to identify

direct targets of HCF-1 that change in expression in mouse hepatocytes, they also identified mitochondrial-related genes as the most significant GO term<sup>27</sup>, suggesting that at least HCF-1 has a highly conserved function in directly regulating mitochondrial gene expression from worms to mammals.

We find that HDA-1 co-occupies many of the same promoters as SET-26 and HCF-1, however whether the connection between HDA-1 with SET-26 and HCF-1 is one of direct binding or mediated by the surrounding chromatin environment is unclear. Interestingly, although SET-26 is an H3K4me3 reader, it can only competently bind H3K4me3 when there are nearby histone acetylation marks<sup>15</sup>, supporting the likelihood that machinery associated with histone acetylation, such as HDA-1, would occupy similar regions of chromatin.

Indeed, we find that it is unlikely that SET-26 or HCF-1 directly alter HDA-1 recruitment to chromatin in somatic cells, but rather we postulate that the three factors occupy the same promoters, with SET-26 and HCF-1 working to mediate gene expression in one direction, while HDA-1 works against them in the other direction. Genes that match this description within our data are enriched for mitochondrial metabolism genes, which are of particular interest given our findings that SET-26 and HCF-1 stabilize each other on and affect expression of mitochondrial genes, and the wide array of literature connecting mitochondrial perturbation with lifespan modulation<sup>2,43,44</sup>. Furthermore, HDA-1 has been shown to be required for activation of the mitoUPR in *C. elegans* and in human cells<sup>13,14</sup>, and to be required for the longevity of a model of mitoUPR-mediated longevity<sup>13</sup>. Thus, it is particularly intriguing to find that many mitoUPR genes are activated in the *set-26(-)* and *hcf-1(-)* long-lived mutants, and their induced expression are reversed in the shorter-lived *set-26(-)* and *hcf-1(-)* mutants on *hda-1* RNAi. It is tempting to speculate that these genes may be the most promising candidates to explain the long lifespan of the *set-26(-)* and *hcf-1(-)* mutants and the decline in lifespan on *hda-1* RNAi. It will be critical for future studies to determine whether these genes are responsible for the

longevity of *set-26(-)* and *hcf-1(-)* mutants in an *hda-1*-dependent manner, and the impact they may have on mitochondrial function in the mutants.

Given the conserved relationship between SET-26 and HCF-1 homologs in humans<sup>23,30</sup> and the conservation of SET-26, HCF-1, and HDA-1 homologs in regulating mitochondria in mammals<sup>13,27,31,42</sup>, it will be interesting to further explore the role between these three factors in mammalian cells, especially in respect to the regulation of mitochondrial gene expression. As all three factors in humans are implicated in neurodevelopment<sup>37,38,45</sup> and cancer<sup>39-41</sup>, and HCF-1's function in cancer has already been linked to the regulation of mitochondrial gene expression<sup>31</sup>, understanding how MLL5, HCF-1, and HDAC1/2 interact and the pathways they regulate in humans could have broad implications for understanding both aging and human disease.

## Methods

### ***C. elegans* maintenance**

Strains with a *glp-1(e2141)* mutant background were maintained at 16 °C, whereas all other strains used were maintained at 20 °C. To maintain worms, animals were well fed on 6-cm nematode growth medium (NGM) plates containing 30 µg/mL streptomycin seeded with 200 µl of a 5X concentrated strep-resistance OP50 overnight culture. In all experiments with the exception of RNAi experiments (which utilize the HT115 bacterial strain), worms were fed OP50. All strains used in this study contained the wild-type (N2H) allele of *fln-2*, a gene which has been shown to be mutated in common *C. elegans* strains and can affect lifespan<sup>46</sup>. See Supplementary Information - Supplementary Table 1 for a list of all strains used in this paper.

### **Lifespan**

Lifespan analysis was conducted similarly as previously described<sup>15</sup>. Specifically, 3-10 gravid adults were allowed to lay embryos on plates with the appropriate bacteria for 2-5 h at the growth temperature of the strain (16 °C for *glp-1(e2141)* strains or 20 °C for all other

strains). The adults were removed and plates containing synchronized embryos were shifted to 25 °C for ~48 h until they reached day 1 of adulthood, which was marked as day 1 for lifespan analysis. 30-35 day 1 adults were then transferred onto 2-3 plates containing either the same bacteria or shifted onto the appropriate bacteria for aging. Specifically, for RNAi experiments using adult *hda-1* RNAi, all worms were grown on the empty vector bacteria “L4440”, then worms were split between L4440 and *hda-1* RNAi at day 1 of adulthood. For lifespan experiments conducted on OP50, worms were grown on stock plates (as described above) containing 5X concentrated live OP50, and then transferred at day 1 of adulthood to NGM plates seeded with 200 µl of a 10X concentrated strep-resistant OP50 overnight culture which had been killed by washing twice with a solution of LB containing 100 µg/mL carbenicillin and 15 µg/mL tetracycline as previously described<sup>8</sup>. Worms used for lifespan were transferred to fresh plates every 1-2 days until the end of their reproductive period and monitored for survival every 2 days until all worms died. The chemical 5-fluoro-2'-deoxyuridine (FUDR) was not used. Worms were scored as dead when they failed to respond to a gentle prod on the head. Worms that exploded, experienced internal hatching of offspring (bagged), or crawled onto the side of the plate were marked as censored on the day of the event. Lifespan data were analyzed with OASIS 2 (<https://sbi.postech.ac.kr/oasis2/>) online survival analysis tool<sup>47</sup>. The Kaplan-Meier estimator was used for re-plotting survival curves in Excel and log-rank tests were utilized to determine whether two lifespans were significantly different. All lifespans were conducted at least twice, and the data displayed in each figure show one representative replicate (See Source Data for all lifespan data).

## RNAi

RNAi was administered by feeding. Briefly, HT115 bacteria expressing double stranded RNA against the gene of interest were obtained from the Ahringer library and verified by Sanger sequencing unless otherwise noted (see “*hda-1* 3' UTR RNAi construction” below). RNAi

bacteria and the control empty vector bacteria, L4440, were grown in overnight cultures containing 100 µg/mL carbenicillin and 15 µg/mL tetracycline at 37 °C for 12-16 h. The overnight cultures were diluted 1:20 in LB containing 100 µg/mL carbenicillin and grown at 37 °C for 2-4 h until an optical density of 0.6-0.8 was reached for all cultures. Cultures were then induced with 1 mM total concentration of IPTG, and grown at 37 °C for an additional 2-3 h. After induction, bacteria were spun down at 3000 rpm for 15-20 min at room temperature and concentrated 50-fold. 200 µl of concentrated bacteria were seeded on 6-cm “RNAi plates” and 1-2 mL were seeded on 15-cm “RNAi plates”, which were NGM plates lacking streptomycin and with the addition of 100 µg/mL ampicillin, 15 µg/mL tetracycline, and 1 mM IPTG. Unless specifically noted as “*hda-1* 3’ UTR RNAi”, “*hda-1* RNAi” refers to the use of the Ahringer RNAi construct.

## CRISPR

The *hcf-1::gfp::3xflag* insertion strain was generated using CRISPR-mediated genome editing as previously described<sup>48</sup>, such that a flexible linker, GFP and 3X FLAG tags were inserted immediately before the endogenous *hcf-1* stop codon in the N2 background. The Dickinson et al. method<sup>48</sup> was used to generate and inject a repair template and guide RNAs, and to select positive hits that were hygromycin-resistant rollers. After initial selection, the self-excising cassette, containing the roller and hygromycin-resistant markers, was removed and successful removal was verified by Sanger sequencing.

The *set-26::ha* insertion strain was generated using CRISPR-mediated genome editing as previously described<sup>15,49,50</sup>, such that an HA tag was inserted immediately before the endogenous *set-26* stop codon in the N2 background.

The *hda-1::gfp::ha* insertion strain was generated by SunyBiotech using CRISPR-mediated genome editing such that the GFP and HA tags were inserted immediately before the endogenous *hda-1* stop codon in the N2 background.

## CUT&RUN

In experiments in which worms were grown on OP50, embryos were collected from full stock plates as previously described<sup>25</sup>. 3000 embryos were seeded per plate on 15-cm NGM plates containing 1mL of a 25-times concentrated overnight culture of streptomycin-resistant OP50. In experiments utilizing *glp-1* RNAi, 150-300 synchronized gravid adults were pre-incubated with RNAi plates seeded with *glp-1* RNAi bacteria overnight for 10-14 h at 20 °C. The next day, the gravid adults were transferred to fresh *glp-1* RNAi plates for 3-6 h at 20 °C, after which the resulting synchronized embryos were washed off of the plates, counted, and seeded, either with 3000 worms per plate for 15-cm plates, or 200 worms per plate for 6-cm plates. For consistency, in experiments with *glp-1* RNAi, control worms laying embryos on L4440 were pre-incubated overnight with L4440 in the same way. Enough embryos were prepared such that 3000 worms were available for each CUT&RUN reaction as previously described<sup>25</sup>. After seeding embryos, plates (either OP50 or RNAi) were incubated at 25 °C for ~48-52 h until the plates were full primarily of young adults. After reaching the young adult stage, worms were washed off plates and CUT&RUN experiments were performed precisely as previously described by us in detail elsewhere<sup>25</sup>, similarly to other standard CUT&RUN protocols<sup>51,52</sup>.

Sequencing libraries were prepared using the NEBNext Ultra II DNA Library Prep Kit for Illumina (NEB, cat. No E7645S and E7335S) and amplified using 14 PCR cycles following the manufacturer's instructions with slight modifications as previously described by us in detail elsewhere<sup>25</sup>. Libraries were submitted for 2x32 paired-end sequencing with an Illumina NextSeq 500 machine. All CUT&RUN experiments were repeated twice, with biological replicates grown and collected separately. See Supplementary Information - Supplementary Table 3 for a detailed list of antibodies used in CUT&RUN experiments.

## CUT&RUN data analysis

Data analysis was performed similarly as described<sup>53</sup>. For detailed information, see Supplementary Information - Supplementary Methods.

## RNA-seq

Embryos were collected from full stock plates of *glp-1(-)*, *glp-1(-);set-26(-)*, and *glp-1(-);hcf-1(-)* strains as described above for CUT&RUN. Embryos were seeded at approximately 60 worms per plate on 6-cm RNAi plates containing L4440 empty vector bacteria and were grown at 25 °C for ~48 h until most worms were young adults. Approximately 300 worms were collected as day 1 adults, and the remaining population was washed off of their plates using M9 buffer containing 0.05% Tween-20 and split evenly onto either fresh L4440 plates or *hda-1* RNAi plates. Two days later, approximately 300 worms were collected from each genotype on either L4440 or *hda-1* RNAi as day 3 adults, and the remaining population was grown until day 12 of adulthood, with one transfer at day 7 onto fresh RNAi plates to ensure worms were well fed. At each collection, worms were washed off of plates with M9 buffer containing 0.05% Tween-20. Worms were settled and washed 1-5 times with M9 buffer, and then were snap frozen in liquid nitrogen in 500 µl of Tri Reagent. Samples were alternatively thawed, vortexed, and re-frozen in liquid nitrogen at least 5 times to break apart worms. 100 µl chloroform was added per tube, and samples were vortexed and then spun at 18,000 rcf for 15 min at 4 °C. The aqueous layer was then transferred to a fresh tube, and 250 µl isopropanol was mixed into each sample. 1 µl GlycoBlue was added and, after a 10 min incubation at RT, samples were spun at 12,000 rcf for 10 min at 4 °C. The supernatant was discarded, and the RNA pellet was washed with 70% ethanol. The pellet was then air dried and dissolved in nuclease-free water. RNA was treated with DNase to remove residual DNA following the instructions from the TURBO DNase kit (Invitrogen, AM1907), and RNA was further purified by ethanol precipitation using 0.1 volumes of 3 M sodium acetate, 2.5 volumes of ice cold 100% ethanol, and 1 µl GlycoBlue overnight at -

80 °C. The following morning, samples were spun at 18,000 rcf for 30 min at 4 °C, pellets were washed twice with ice cold 75% ethanol, and the pellet was air dried and dissolved in nuclease-free water. RNA-seq libraries were prepared with the QuantSeq 3' mRNA-Seq Library Prep Kit (Lexogen) following the manufacturer's instructions beginning with 315 ng RNA from each sample and using 13 PCR cycles. Libraries were quantified with Qubit and quality checked using Bioanalyzer and then submitted for single-end 86bp sequencing with an Illumina NextSeq 500 machine.

### **RNA-seq data analysis**

In the linux environment, adaptor sequences were trimmed and low quality reads were filtered out from sequencing files using Trim Galore! (v0.6.5) , which utilizes Cutadapt (v3.4)<sup>54</sup> and FastQC (v0.11.8), with the settings `-q 20 -fastqc`. Trimmed sequencing files were then aligned to the ce11/WBcel235 *C. elegans* reference genome using STAR (v2.7.9a)<sup>55</sup> with the options `-runThreadN 2 -quantMode GeneCounts --outFilterMultiMapNmax 1 -outFilterMismatchNmax 2 -outSAMtype BAM SortedByCoordinate`. The resulting tab delimited text files containing read count per gene, with column 3 (the middle column of counts) representing the correct counts for 3' RNA-seq data, were used to create a matrix of gene expression to compare multiple samples. Matrices contained either all genotypes at the same age on the same bacteria (e.g. *glp-1(-)*, *glp-1(-);set-26(-)*, and *glp-1(-);hcf-1(-)* on L4440 at Day 3) or the same genotype at the same age on different bacteria (e.g. *glp-1* on L4440 and *hda-1* RNAi), depending on whether the goal was to identify genes differentially expressed in the longevity mutants or genes dependent on *hda-1* in one genotype. The matrices were uploaded into RStudio and used as input to DESeq2 (v1.34.0)<sup>56</sup>. Genes with low read counts were pre-filtered out before differential analysis, and only genes that had more than 10 read counts in at least 2 samples were kept for analysis. PCA plots were generated using the 'vst' transformation function in DESeq2 and the 'plotPCA' function with default settings, followed by the 'ggplot'

function in ggplot2 (v3.3.6)<sup>57</sup>. DESeq2 was used to find the differentially expressed genes either by genotype or condition (*hda-1* RNAi) using the standard DESeq command. Only the genes reaching an adjusted p value of less than 0.05 were kept and considered significant. Normalized counts for particular genes of interest were plotted using the 'plotCounts' function in DESeq2. Genes sets in each genotype were compared to each other or to CUT&RUN genes using BioVenn ([www.biovenn.nl](http://www.biovenn.nl))<sup>58</sup>, and the significance of overlapping genes were determined by Fisher's exact test calculated in RStudio. WormCat 2.0 ([www.wormcat.com](http://www.wormcat.com)) was used for gene ontology enrichment analysis, where the p values are determined by Fisher's test with FDR correction<sup>59</sup>.

To generate heatmaps using RNA-seq data, gene expression matrices were uploaded into DESeq2 as described above, except lowly expressed genes were not pre-filtered. DESeq2 was again used to find differentially expressed genes as described above, and the log<sub>2</sub> fold change values were extracted from the DESeq2 result table for each gene to be plotted in the heatmap. Heatmaps were plotted with the 'Heatmap' function in the ComplexHeatmap package (v2.10.0)<sup>60</sup> with the options 'cluster\_rows = T, cluster\_columns = F, show\_row\_names = FALSE, row\_dend\_reorder = TRUE, na\_col = "black"'. To split a heatmap, the option 'split = 3' was added and the genes from each clustered section were extracted using the 'row\_order' function in ComplexHeatmap.

### **Immunoblotting and quantification**

300-1000 synchronized adult worms were washed off of plates with M9 buffer containing 0.05% Tween-20. Worms were settled and washed 1-5 times with M9 buffer, and then snap frozen in liquid nitrogen in minimal M9 buffer. Immunoblots were run as previously described<sup>15</sup>. Samples were boiled for 7 min at 100 °C in an equal volume of 2X SDS sample buffer and run through an SDS page gel containing 8% acrylamide. After separation, samples were transferred to a nitrocellulose membrane for 1 h at 4 °C. The membrane was then blocked with Tris-

buffered saline containing 0.1% tween (TBST) and 5% BSA, washed with TBST and incubated overnight at 4 °C with primary antibody (1:1000 for FLAG; 1:2000 for H3) diluted in TBST + 5% BSA. The membrane was then washed again with TBST 3 times, and incubated with a fluorescent secondary antibody (1:5000) at RT for 1.5-2.5 h in the dark. Membranes were washed 3 times with TBST, once with TBS, and then imaged using the ChemiDoc MP Imaging System. Immunoblots were repeated 2-3 times. Fluorescence of the target protein was normalized to H3 fluorescence using the BioRad Image Lab Software, and then fold change was calculated between conditions. Statistical significance of fold change compared to control was analyzed using one-tailed or two-tailed t-tests as specified in figure legends. See Supplementary Information - Supplementary Table 3 for a detailed list of antibodies used in immunoblotting experiments.

### ***hda-1* 3' UTR RNAi construction**

The *hda-1* 3' UTR RNAi construct was designed to target a unique 774 bp region in the 3' UTR of *hda-1*. This region in *hda-1* was amplified from N2 genomic DNA with primers containing restriction digest sites for EcoO109I and SacI-HF restriction enzymes. Purified PCR products and purified DNA from miniprep of the L4440 vector were digested with EcoO109I and SacI-HF in rCutSmart™ (NEB) buffer for 1 h or 16 h at 37 °C. The digested products were purified and ligated together using T4 DNA ligase (NEB). The ligation product was then retransformed into high-efficiency 5-alpha competent *E. coli* cells (NEB) which were grown overnight at 37 °C. Colonies were grown for 12-16 h overnight at 37 °C in LB containing 100 µg/mL carbenicillin and plasmids were purified by miniprep and verified with Sanger sequencing. 1 µl of the correct plasmid was then retransformed into homemade HT115 competent cells and used for RNAi. See Supplementary Information - Supplementary Table 2 for primer sequences.

## qRT-PCR

For qRT-PCR, 50-300 worms were collected at day 3 of adulthood on L4440 or *hda-1* RNAi, with *hda-1* RNAi initiated on day 1 of adulthood. Samples were frozen and RNA isolated, DNase-treated, and purified as described for RNA-seq above. cDNA was synthesized using qScript cDNA SuperMix from Quantabio following manufacturer's instructions, then 1  $\mu$ l RNase H was added to the reaction and incubated for 20 min at 37 °C to remove residual RNA. qRT-PCR reactions were performed in triplicate on a LightCycler 480 II machine in 10  $\mu$ l reactions containing 2  $\mu$ l of 10-fold diluted cDNA, 1  $\mu$ l of 5  $\mu$ M primers, and 7  $\mu$ l of Taq mix containing a SybrGreen mix, dNTPs, and hot start Taq. Ct values were obtained using the LightCycler 480 Software high sensitivity setting. Triplicate Ct values were averaged, then normalized to first a housekeeping gene (*ama-1*) and then control samples using the  $2^{-\Delta\Delta Ct}$  method<sup>61</sup> to compute fold change of *hda-1* with *hda-1* RNAi compared to empty vector bacteria. Two biological replicates were conducted for each qRT-PCR experiment. Statistical significance of fold change compared to control was analyzed using one-tailed t-tests. See Supplementary Information - Supplementary Table 2 for primer sequences.

## Statistics and reproducibility

Statistical analyses were performed in Microsoft® Excel (v16.66.1) for immunoblotting and qRT-PCR experiments, in OASIS 2<sup>47</sup> for lifespan analyses, in WormCat 2.0<sup>59</sup> for gene ontology analyses, and in RStudio (v2022.02.0+443) for all other analyses. The R packages used for differential analyses in CUT&RUN and RNA-seq data sets are included in the methods section and Supplementary Methods. All experiments were repeated with at least two biological replicates with similar results. The details of types of statistical analyses and p value cutoffs for each experiment are included in the corresponding figure legend, and the raw data including sample size and statistical analysis for each figure are included in the Source Data file.

## Data availability

The source data for Figs. 1a, 5a-b, and Supplementary Figures 1b, c, e, f, h, i, 3c-e, 5a-c, e, g, 7a, b, e, and f are provided in the Source Data file. Lists of peaks, differentially expressed genes, and overlapping gene sets used to generate Venn Diagrams are provided in Supplementary Data files.

## References

1. Cui, M. & Han, M. Roles of chromatin factors in *C. elegans* development. *WormBook* 1–16 (2007).
2. López-Otín, C., Blasco, M. A., Partridge, L., Serrano, M. & Kroemer, G. The hallmarks of aging. *Cell* **153**, 1194–1217 (2013).
3. Wang, K. *et al.* Epigenetic regulation of aging: implications for interventions of aging and diseases. *Signal Transduct Target Ther* **7**, 374 (2022).
4. Wenzel, D., Palladino, F. & Jedrusik-Bode, M. Epigenetics in *C. elegans*: facts and challenges. *Genesis* **49**, 647–661 (2011).
5. Li, J. *et al.* *Caenorhabditis elegans* HCF-1 functions in longevity maintenance as a DAF-16 regulator. *PLoS Biol.* **6**, e233 (2008).
6. Jin, C. *et al.* Histone demethylase UTX-1 regulates *C. elegans* life span by targeting the insulin/IGF-1 signaling pathway. *Cell Metab.* **14**, 161–172 (2011).
7. Maures, T. J., Greer, E. L., Hauswirth, A. G. & Brunet, A. The H3K27 demethylase UTX-1 regulates *C. elegans* lifespan in a germline-independent, insulin-dependent manner. *Aging Cell* **10**, 980–990 (2011).
8. Ni, Z., Ebata, A., Alipanahramandi, E. & Lee, S. S. Two SET domain containing genes link epigenetic changes and aging in *Caenorhabditis elegans*. *Aging Cell* **11**, 315–325 (2012).
9. Merkwirth, C. *et al.* Two Conserved Histone Demethylases Regulate Mitochondrial Stress-

- Induced Longevity. *Cell* **165**, 1209–1223 (2016).
10. Singh, A. *et al.* A chromatin modifier integrates insulin/IGF-1 signalling and dietary restriction to regulate longevity. *Aging Cell* **15**, 694–705 (2016).
  11. Tian, Y. *et al.* Mitochondrial Stress Induces Chromatin Reorganization to Promote Longevity and UPR(mt). *Cell* **165**, 1197–1208 (2016).
  12. Han, S. *et al.* Mono-unsaturated fatty acids link H3K4me3 modifiers to *C. elegans* lifespan. *Nature* **544**, 185–190 (2017).
  13. Shao, L.-W. *et al.* Histone deacetylase HDA-1 modulates mitochondrial stress response and longevity. *Nat. Commun.* **11**, 4639 (2020).
  14. Zhu, D. *et al.* NuRD mediates mitochondrial stress-induced longevity via chromatin remodeling in response to acetyl-CoA level. *Sci Adv* **6**, eabb2529 (2020).
  15. Wang, W. *et al.* SET-9 and SET-26 are H3K4me3 readers and play critical roles in germline development and longevity. *Elife* **7**, (2018).
  16. Zargar, Z. & Tyagi, S. Role of host cell factor-1 in cell cycle regulation. *Transcription* **3**, 187–192 (2012).
  17. Rizki, G. *et al.* The evolutionarily conserved longevity determinants HCF-1 and SIR-2.1/SIRT1 collaborate to regulate DAF-16/FOXO. *PLoS Genet.* **7**, e1002235 (2011).
  18. Lee, S. *et al.* Epigenetic regulation of histone H3 serine 10 phosphorylation status by HCF-1 proteins in *C. elegans* and mammalian cells. *PLoS One* **2**, e1213 (2007).
  19. Shahbazian, M. D. & Grunstein, M. Functions of site-specific histone acetylation and deacetylation. *Annu. Rev. Biochem.* **76**, 75–100 (2007).
  20. Shi, Y. & Mello, C. A CBP/p300 homolog specifies multiple differentiation pathways in *Caenorhabditis elegans*. *Genes Dev.* **12**, 943–955 (1998).
  21. Dufourcq, P. *et al.* Functional requirement for histone deacetylase 1 in *Caenorhabditis elegans* gonadogenesis. *Mol. Cell. Biol.* **22**, 3024–3034 (2002).
  22. Zhu, L., Zhou, Q., He, L. & Chen, L. Mitochondrial unfolded protein response: An emerging

- pathway in human diseases. *Free Radic. Biol. Med.* **163**, 125–134 (2021).
23. Zhou, P. *et al.* Mixed lineage leukemia 5 (MLL5) protein regulates cell cycle progression and E2F1-responsive gene expression via association with host cell factor-1 (HCF-1). *J. Biol. Chem.* **288**, 17532–17543 (2013).
  24. Kimble, J. & Hirsh, D. The postembryonic cell lineages of the hermaphrodite and male gonads in *Caenorhabditis elegans*. *Dev. Biol.* **70**, 396–417 (1979).
  25. Emerson, F. J. & Lee, S. S. CUT&RUN for Chromatin Profiling in *Caenorhabditis elegans*. *Curr Protoc* **2**, e445 (2022).
  26. Michaud, J. *et al.* HCFC1 is a common component of active human CpG-island promoters and coincides with ZNF143, THAP11, YY1, and GABP transcription factor occupancy. *Genome Res.* **23**, 907–916 (2013).
  27. Minocha, S. *et al.* Rapid Recapitulation of Nonalcoholic Steatohepatitis upon Loss of Host Cell Factor 1 Function in Mouse Hepatocytes. *Mol. Cell. Biol.* **39**, (2019).
  28. Zhu, L. J. *et al.* ChIPpeakAnno: a Bioconductor package to annotate ChIP-seq and ChIP-chip data. *BMC Bioinformatics* **11**, 237 (2010).
  29. Ali, M. *et al.* Molecular basis for chromatin binding and regulation of MLL5. *Proc. Natl. Acad. Sci. U. S. A.* **110**, 11296–11301 (2013).
  30. Lee, K.-H. *et al.* MLL5, a histone modifying enzyme, regulates androgen receptor activity in prostate cancer cells by recruiting co-regulators, HCF1 and SET1. *BMB Rep.* **53**, 634–639 (2020).
  31. Popay, T. M. *et al.* MYC regulates ribosome biogenesis and mitochondrial gene expression programs through its interaction with host cell factor-1. *Elife* **10**, (2021).
  32. Rincon-Arano, H., Halow, J., Delrow, J. J., Parkhurst, S. M. & Groudine, M. UpSET recruits HDAC complexes and restricts chromatin accessibility and acetylation at promoter regions. *Cell* **151**, 1214–1228 (2012).
  33. De Vaux, V. *et al.* The *Caenorhabditis elegans* LET-418/Mi2 plays a conserved role in

- lifespan regulation. *Aging Cell* **12**, 1012–1020 (2013).
34. Edwards, C. *et al.* D-beta-hydroxybutyrate extends lifespan in *C. elegans*. *Aging* **6**, 621–644 (2014).
  35. Wang, Z. *et al.* Genome-wide mapping of HATs and HDACs reveals distinct functions in active and inactive genes. *Cell* **138**, 1019–1031 (2009).
  36. Yoneda, T. *et al.* Compartment-specific perturbation of protein handling activates genes encoding mitochondrial chaperones. *J. Cell Sci.* **117**, 4055–4066 (2004).
  37. Li, Y.-J. *et al.* KMT2E Haploinsufficiency Manifests Autism-Like Behaviors and Amygdala Neuronal Development Dysfunction in Mice. *Mol. Neurobiol.* (2022) doi:10.1007/s12035-022-03167-w.
  38. Jolly, L. A. *et al.* HCFC1 loss-of-function mutations disrupt neuronal and neural progenitor cells of the developing brain. *Hum. Mol. Genet.* **24**, 3335–3347 (2015).
  39. Zhang, X., Novera, W., Zhang, Y. & Deng, L.-W. MLL5 (KMT2E): structure, function, and clinical relevance. *Cell. Mol. Life Sci.* **74**, 2333–2344 (2017).
  40. Glinsky, G. V., Berezovska, O. & Glinskii, A. B. Microarray analysis identifies a death-from-cancer signature predicting therapy failure in patients with multiple types of cancer. *J. Clin. Invest.* **115**, 1503–1521 (2005).
  41. Li, Y. & Seto, E. HDACs and HDAC Inhibitors in Cancer Development and Therapy. *Cold Spring Harb. Perspect. Med.* **6**, (2016).
  42. Tasdogan, A. *et al.* DNA Damage-Induced HSPC Malfunction Depends on ROS Accumulation Downstream of IFN-1 Signaling and Bid Mobilization. *Cell Stem Cell* **19**, 752–767 (2016).
  43. Lee, S. S. *et al.* A systematic RNAi screen identifies a critical role for mitochondria in *C. elegans* longevity. *Nat. Genet.* **33**, 40–48 (2003).
  44. Dillin, A. *et al.* Rates of behavior and aging specified by mitochondrial function during development. *Science* **298**, 2398–2401 (2002).

45. D'Mello, S. R. Histone deacetylases 1, 2 and 3 in nervous system development. *Curr. Opin. Pharmacol.* **50**, 74–81 (2020).
46. Zhao, Y., Wang, H., Poole, R. J. & Gems, D. A fln-2 mutation affects lethal pathology and lifespan in *C. elegans*. *Nat. Commun.* **10**, 5087 (2019).
47. Han, S. K. *et al.* OASIS 2: online application for survival analysis 2 with features for the analysis of maximal lifespan and healthspan in aging research. *Oncotarget* **7**, 56147–56152 (2016).
48. Dickinson, D. J., Pani, A. M., Heppert, J. K., Higgins, C. D. & Goldstein, B. Streamlined Genome Engineering with a Self-Excising Drug Selection Cassette. *Genetics* **200**, 1035–1049 (2015).
49. Friedland, A. E. *et al.* Heritable genome editing in *C. elegans* via a CRISPR-Cas9 system. *Nat. Methods* **10**, 741–743 (2013).
50. Paix, A. *et al.* Scalable and versatile genome editing using linear DNAs with microhomology to Cas9 Sites in *Caenorhabditis elegans*. *Genetics* **198**, 1347–1356 (2014).
51. Skene, P. J. & Henikoff, S. An efficient targeted nuclease strategy for high-resolution mapping of DNA binding sites. *Elife* **6**, (2017).
52. Skene, P. J., Henikoff, J. G. & Henikoff, S. Targeted in situ genome-wide profiling with high efficiency for low cell numbers. *Nat. Protoc.* **13**, 1006–1019 (2018).
53. Li, C.-L. *et al.* Region-specific H3K9me3 gain in aged somatic tissues in *Caenorhabditis elegans*. *PLoS Genet.* **17**, e1009432 (2021).
54. Martin, M. Cutadapt removes adapter sequences from high-throughput sequencing reads. *EMBnet.journal* **17**, 10–12 (2011).
55. Dobin, A. *et al.* STAR: ultrafast universal RNA-seq aligner. *Bioinformatics* **29**, 15–21 (2013).
56. Love, M. I., Huber, W. & Anders, S. Moderated estimation of fold change and dispersion for RNA-seq data with DESeq2. *Genome Biol.* **15**, 550 (2014).
57. Wickham, H. Ggplot2: elegant graphics for data analysis Springer-Verlag, New York: ISBN

978-3-319-24277-4. (2016).

58. Hulsen, T., de Vlieg, J. & Alkema, W. BioVenn - a web application for the comparison and visualization of biological lists using area-proportional Venn diagrams. *BMC Genomics* **9**, 488 (2008).
59. Holdorf, A. D. *et al.* WormCat: An Online Tool for Annotation and Visualization of *Caenorhabditis elegans* Genome-Scale Data. *Genetics* **214**, 279–294 (2020).
60. Gu, Z., Eils, R. & Schlesner, M. Complex heatmaps reveal patterns and correlations in multidimensional genomic data. *Bioinformatics* **32**, 2847–2849 (2016).
61. Livak, K. J. & Schmittgen, T. D. Analysis of relative gene expression data using real-time quantitative PCR and the  $2^{-\Delta\Delta C(T)}$  Method. *Methods* **25**, 402–408 (2001).

## Acknowledgements

Thank you to members of the Lee Lab for helpful suggestions and discussions in all aspects of experimental design and data analysis. Thank you to Rada Omanovic for buffer and plate preparation. Thank you to Dr. Wenke Wang for strain construction and Dr. Meng-Qui Dong and Dr. Christian Riedel for assistance with the IP-Mass Spec. Thank you to the Cornell University Institute of Biotechnology and Genomics Facility for Illumina sequencing and computing power. Some strains were supplied by the *Caenorhabditis* Genetics Center (CGC), and the work was supported by NIH funding to S.S.L. (R01 AG024425) and NSF GRFP funding to F.J.E. (DGE-1650441).

## Author Contributions

F.J.E. and S.S.L. designed the study and wrote the paper. L.Y.L. and C.C. both carried out a lifespan experiment and qRT-PCR experiment. M.Z. performed the IP-Mass Spec analysis.

F.J.E. carried out all other experiments and data analysis. S.S.L. secured funding and supervised the experimental plans.

### **Competing Interests Statement**

The authors declare no competing interests.

### **Figures**

**Fig. 1**

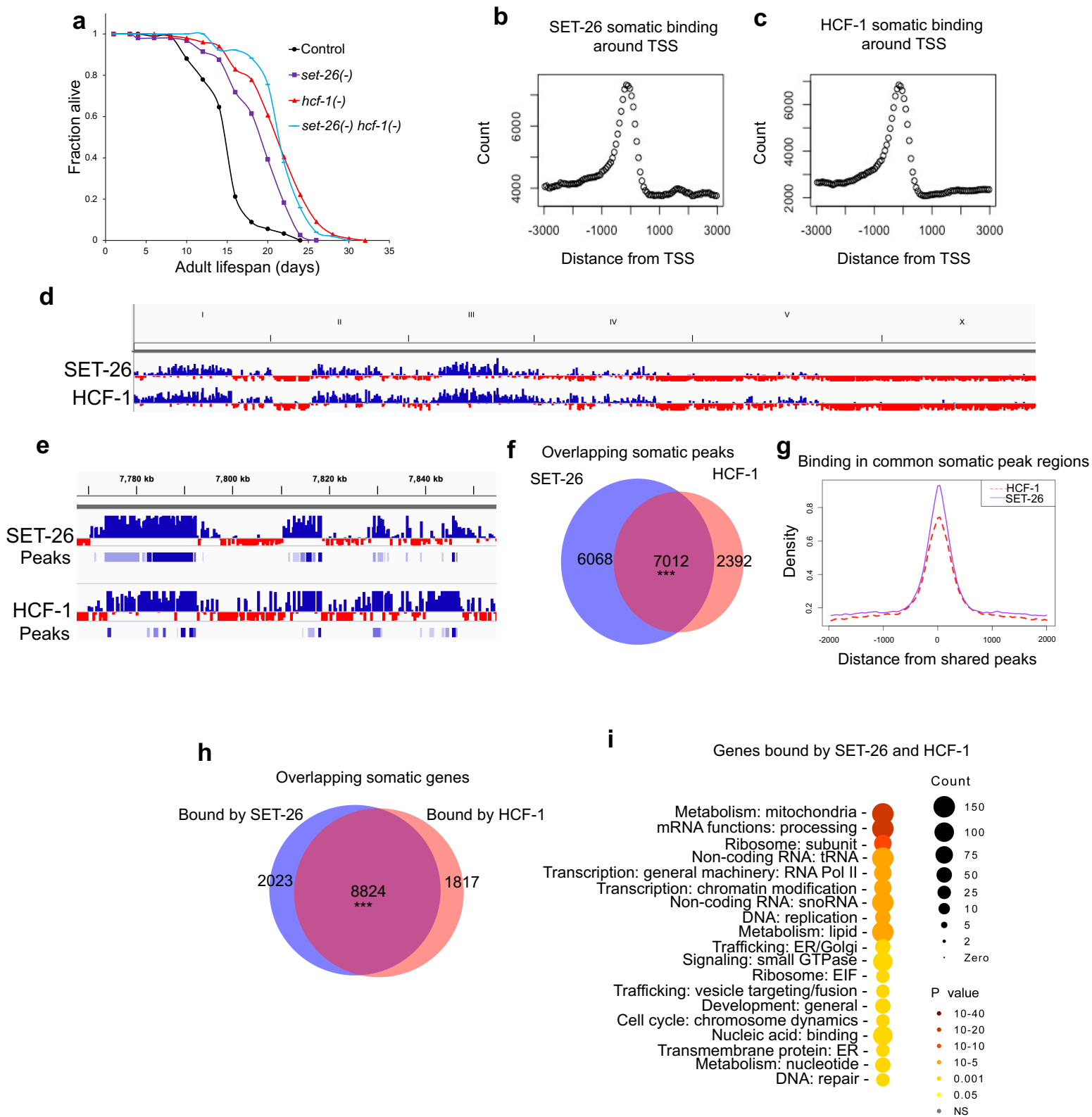


**Fig. 1: SET-26 and HCF-1 operate in the same genetic pathway to modulate lifespan and**

**have overlapping binding profiles at chromatin. a** Survival curves for wildtype controls, *set-26(-)*, *hcf-1(-)*, and *set-26(-) hcf-1(-)* double mutants from one representative experiment.

Quantitative data are provided in Source Data. **b-c** Distribution of somatic (b) SET-26 or (c)

HCF-1 peaks relative to the transcription start sites (TSS) of associated genes within 3kb. Count represents the number of somatic peaks within each bin. Data were obtained from CUT&RUN

assays in either *glp-1(-);set-26::ha* or *glp-1(-);hcf-1::gfp::3xflag* tagged strains. **d** Screenshot

from the Integrated Genomics Viewer (IGV) showing a genome-wide view of somatic SET-26 or HCF-1 binding. Binding is displayed as normalized log<sub>2</sub> signal, where blue represents

enrichment, and red represents depletion, of factor binding relative to control. **e** shows the same binding data as in (d) but for a portion of Chromosome IV. Binding is displayed on the top track,

and peaks called by MACS2 are displayed on the bottom track, where the darker blue

represents more statistically significant peaks as determined by MACS2. **f** Venn diagram

showing somatic SET-26 and HCF-1 peaks in the *glp-1(-)* mutant background, and 7,012 peaks

showing an overlap of 1bp or more. **g** Metaplots of normalized SET-26 and HCF-1 binding

signals within the 7,012 overlapping peak regions identified in (f). **h** Venn diagram showing the

number of genes associated with somatic SET-26 or HCF-1 binding, and 8,824 genes that are commonly bound by both factors. **i** Gene ontology (GO) term analysis for the 8,824 genes

bound by both SET-26 and HCF-1 in somatic cells as determined by Wormcat. In (f and h) \*\*\*

indicates  $p < 1 \times 10^{-15}$  and the overlap is higher than expected by chance, as calculated by

hypergeometric test for peak overlap (in f) and Fisher's Test for gene overlap (in h). In (i),

Wormcat *p* values are determined by Fisher test with FDR correction. Peaks and gene sets are

provided in Supplementary Data 1.

**Fig. 2**

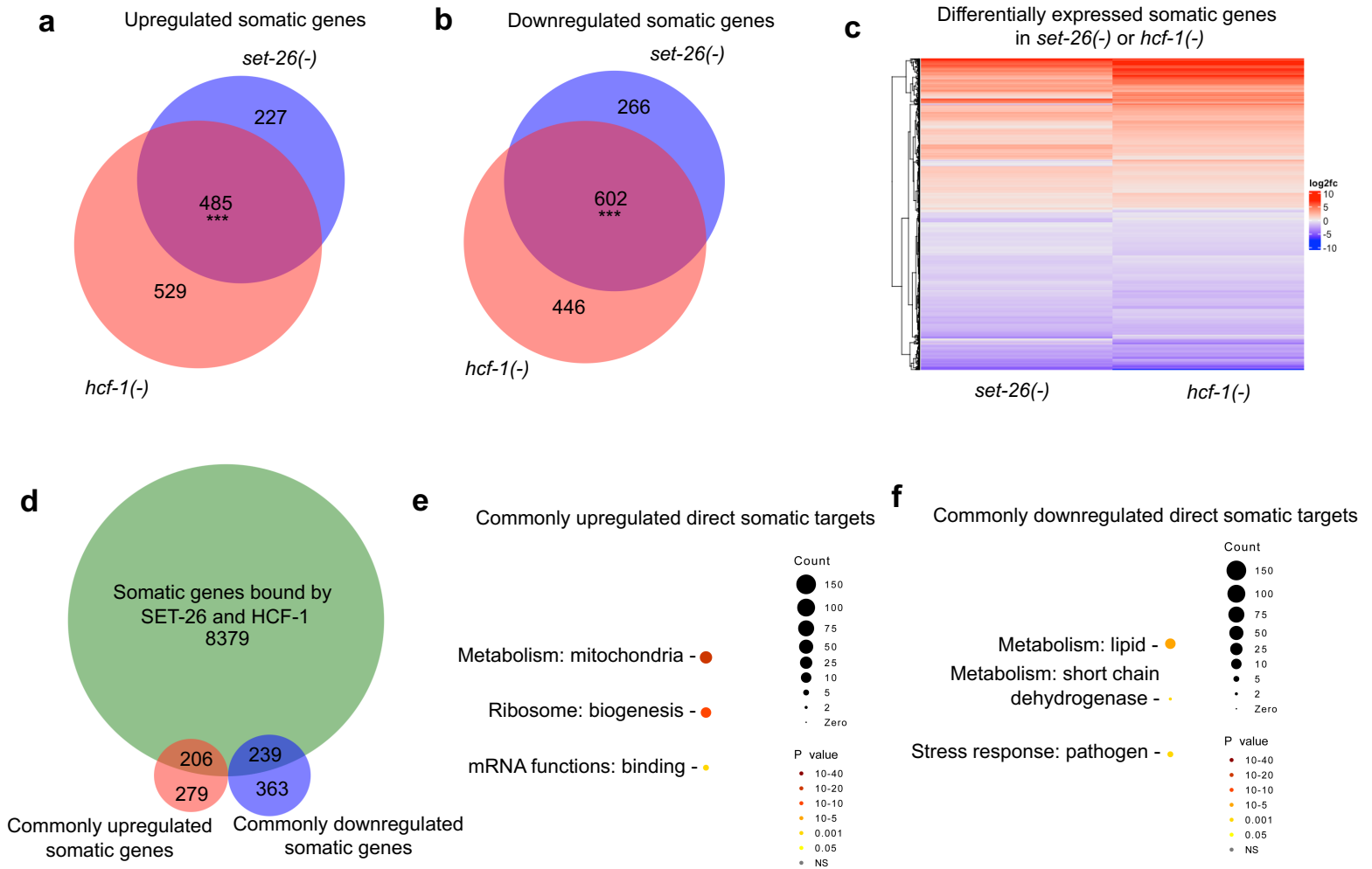


**Fig. 2: SET-26 and HCF-1 regulate a common set of genes. a-b** Venn diagrams showing genes (a) upregulated or (b) downregulated in RNA expression in germline-less day 1 adult *glp-1(-);set-26(-)* or *glp-1(-);hcf-1(-)* double mutants compared to *glp-1(-)* single mutants and the overlapping 485 upregulated, or 602 downregulated genes with significant expression changes in both mutants. **c** Heatmap showing hierarchical clustering of all differentially expressed genes in either *glp-1(-);set-26(-)* or *glp-1(-);hcf-1(-)* double mutants compared to *glp-1(-)* single mutants; The log<sub>2</sub> fold change of RNA expression in each double mutant versus control was used for the clustering analysis and is shown as indicated on the scale. **d** Venn diagram showing the genes bound by SET-26 and HCF-1 as determined in Fig. 1h and the genes commonly upregulated or downregulated in RNA expression when *set-26* or *hcf-1* is inactivated as determined in (a and b). 445 genes are bound by both SET-26 and HCF-1 and show significant RNA expression change in both mutants. **e-f** GO term analysis by Wormcat of SET-26 and HCF-1 direct somatic targets that are (e) upregulated (206) or (f) downregulated (239) in RNA expression in (d). In (a) and (b), \*\*\* indicates  $p < 1 \times 10^{-15}$  and the overlap is higher than expected by chance, as calculated by Fisher's Test. In (e) and (f), Wormcat *p* values are determined by Fisher test with FDR correction. Gene sets are provided in Supplementary Data 2.

**Fig. 3**

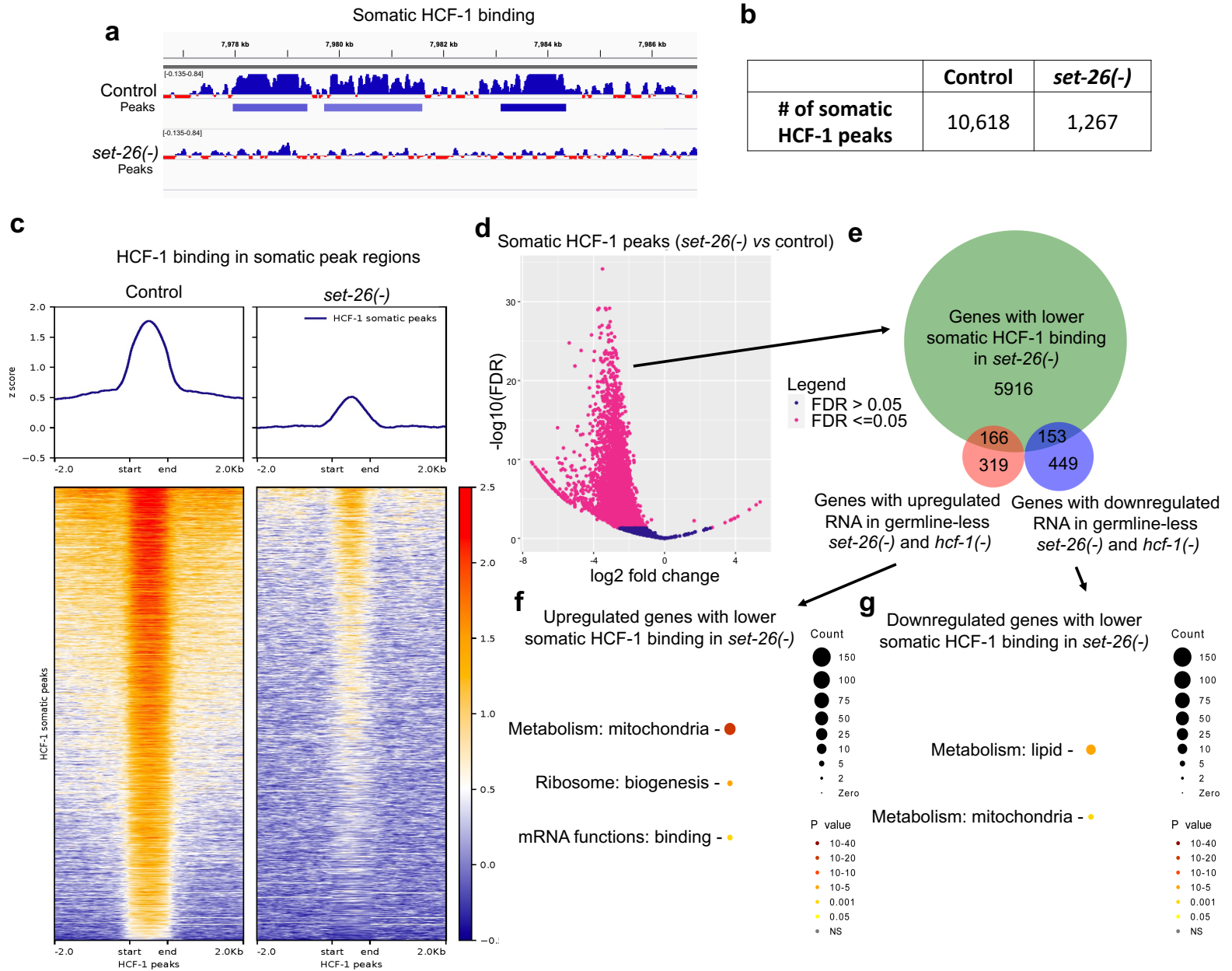


**Fig. 3: HCF-1 recruitment to chromatin in somatic cells requires SET-26.** **a** Screenshot from IGV shows normalized somatic HCF-1 binding and peak calls in a portion of Chromosome V (captured by CUT&RUN of *hcf-1::gfp::3xflag* worms) in control worms or *set-26(-)* mutants grown on *gfp-1* RNAi. **b** Number of HCF-1 peaks called in combined replicates of controls or *set-26(-)* mutants grown on *gfp-1* RNAi. **c** Metaplot (top) and heatmap (bottom) of z-scores representing normalized HCF-1 signal in somatic HCF-1 binding sites and surrounding 2kb up- and downstream in either controls or *set-26(-)* mutants grown on *gfp-1* RNAi. **d** Volcano plot of HCF-1 binding regions determined by DiffBind to be significantly different (pink, FDR  $\leq 0.05$ ) or unchanged (blue, FDR  $>0.05$ ) in *set-26(-)* mutants compared to controls grown on *gfp-1* RNAi. DiffBind FDR values are calculated using DESeq2. **e** Venn diagram of genes with significantly lower HCF-1 binding in *set-26(-)* mutants grown on *gfp-1* RNAi (as determined in **d**) and the overlap with genes up- or downregulated in RNA expression in germline-less *set-26(-)* and *hcf-1(-)* mutants (from Fig. 2a and b). **f-g** Wormcat GO enrichment analysis for genes with lower HCF-1 binding in *set-26(-)* mutants on *gfp-1* RNAi that are either (**f**) upregulated or (**g**) downregulated in RNA expression in both *set-26(-)* and *hcf-1(-)* germline-less mutants (from **e**). Wormcat *p* values are determined by Fisher test with FDR correction. Gene sets and differential peaks are provided in Supplementary Data 2 and 3.

**Fig. 4**

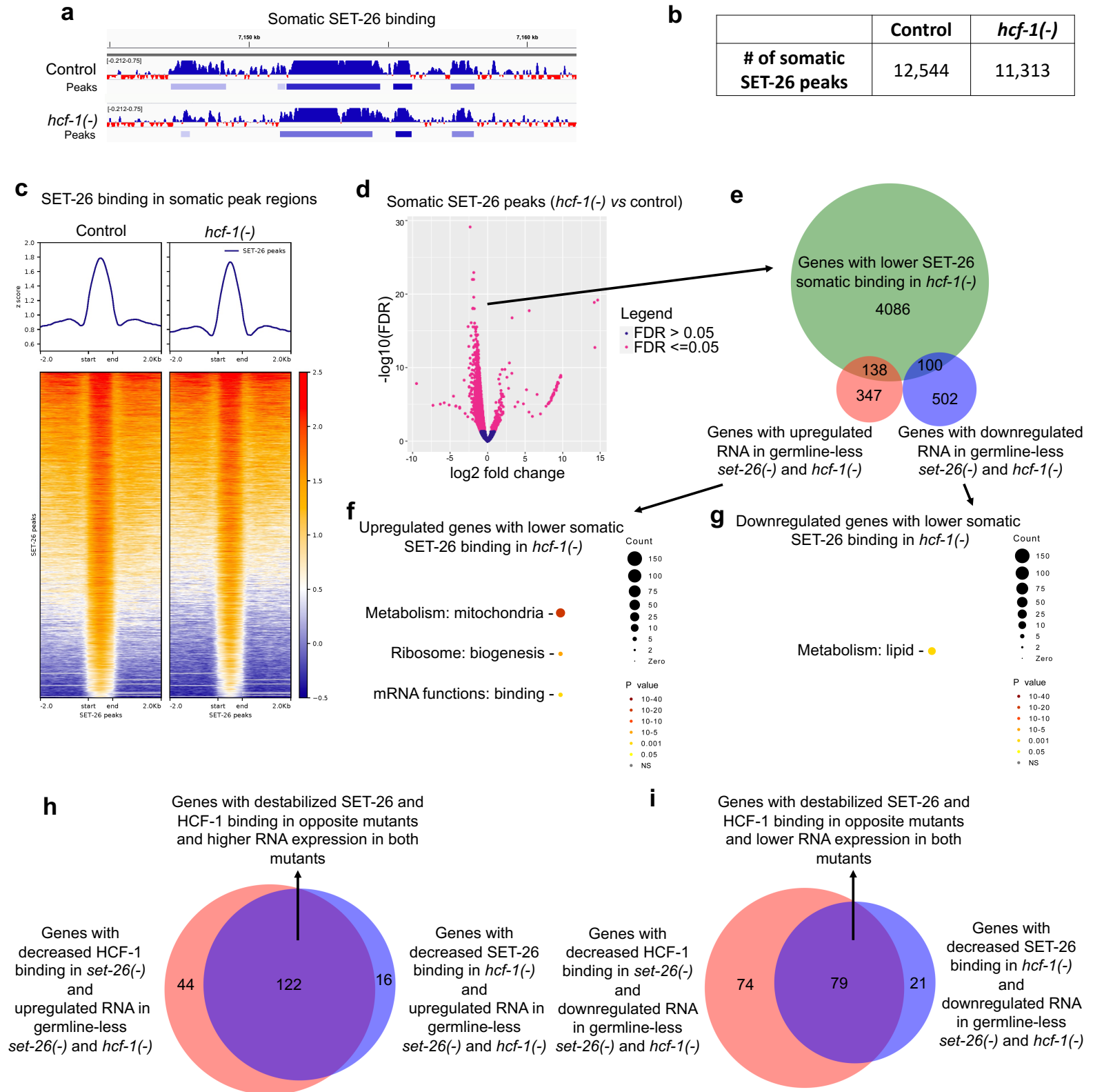


**Fig. 4: HCF-1 is dispensable for most SET-26 recruitment genome-wide, but facilitates**

**SET-26 binding at a subset of somatic binding sites. a** Screenshot from IGV shows

normalized somatic SET-26 binding and peak calls in a portion of Chromosome II (captured by

CUT&RUN of *set-26::ha* worms) in controls or *hcf-1(-)* mutants grown on *glp-1* RNAi. **b** Number

of SET-26 peaks called in combined replicates of controls or *hcf-1(-)* mutants grown on *glp-1*

RNAi. **c** Metaplot (top) and heatmap (bottom) of z-scores representing normalized SET-26

signal in somatic SET-26 binding sites and surrounding 2kb up- and downstream in either

controls or *hcf-1(-)* mutants grown on *glp-1* RNAi. **d** Volcano plot of SET-26 binding regions

determined by DiffBind to be significantly different (pink, FDR  $\leq 0.05$ ) or unchanged (blue, FDR

$>0.05$ ) in *hcf-1(-)* mutants compared to controls grown on *glp-1* RNAi. DiffBind FDR values are

calculated using DESeq2. **e** Venn diagram showing the overlap of the somatic genes with

significantly lower SET-26 binding in *hcf-1(-)* mutants grown on *glp-1* RNAi (as determined in **d**)

and those with up- or downregulated RNA expression in germline-less *set-26(-)* and *hcf-1(-)*

mutants (as seen in Fig. 2a and b). **f-g** Wormcat GO enrichment analysis for genes with lower

SET-26 binding in *hcf-1(-)* mutants on *glp-1* RNAi that are either **(f)** upregulated or **(g)**

downregulated in RNA expression in *set-26(-)* and *hcf-1(-)* mutants (from **e**). Wormcat *p* values

are determined by Fisher test with FDR correction. **h-i** Venn diagram showing the number of

genes with decreased SET-26 or HCF-1 binding in the opposite mutant and the **(h)** 122 that

overlap and are upregulated or **(i)** 79 that overlap and are downregulated in RNA expression in

both mutants as determined in **(e)** and Fig. 3e. Gene sets and differential peaks are provided in

Supplementary Data 2 and 3.

**Fig. 5**

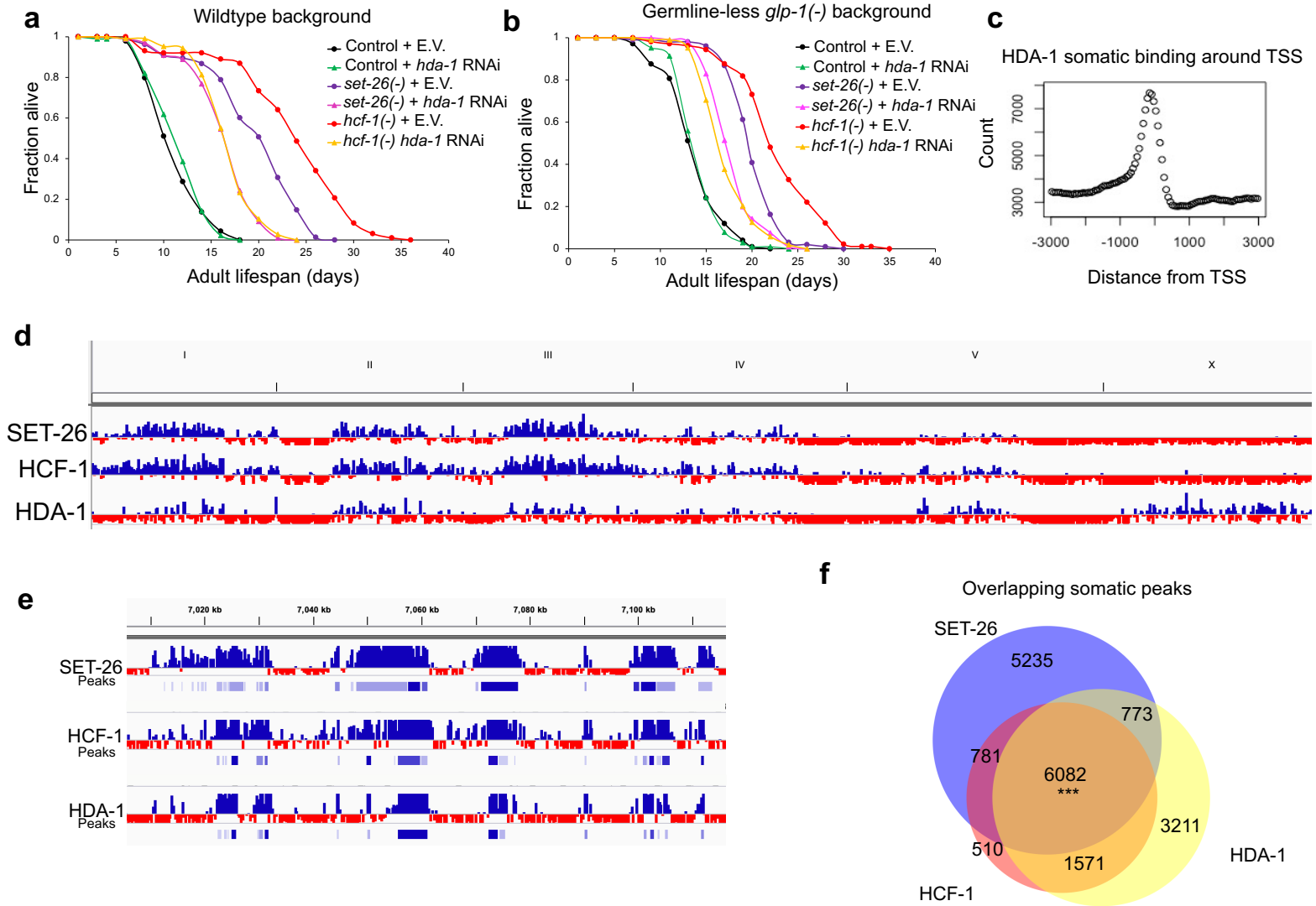


**Fig. 5: HDA-1 is required for the full longevity of *set-26(-)* and *hcf-1(-)* mutants and co-**

**occupies many binding sites with SET-26 and HCF-1. a** Survival curves for wildtype controls, *set-26(-)*, and *hcf-1(-)* mutants on E.V. control RNAi and *hda-1* RNAi from one representative experiment. **b** Survival curves for *glp-1(-)* germline-less controls, *glp-1(-);set-26(-)*, and *glp-1(-);hcf-1(-)* mutants on E.V. control RNAi and *hda-1* RNAi from one representative experiment. In all experiments, *hda-1* RNAi was initiated on day 1 of adulthood to avoid developmental defects caused by initiating *hda-1* RNAi from egglay. **c** Distribution of somatic HDA-1 peaks relative to the transcription start sites (TSS) of associated genes within 3kb. Count represents the number of somatic peaks within each bin. Data were obtained from CUT&RUN assays in the *glp-1(-);hda-1::gfp::ha* tagged strain. **d-e** Screenshots from IGV show normalized somatic SET-26, HCF-1 (as in Fig. 1), and HDA-1 binding either in a **(d)** whole genome view, or a **(e)** close-up of a section of Chromosome II, with peaks called by MACS2 underneath the signal track for each factor. **f** Venn diagram showing somatic SET-26, HCF-1, and HDA-1 peaks in the *glp-1(-)* mutant background and 6,082 peaks that overlap by 1bp or more. In **(f)**, \*\*\* indicates  $p < 1 \times 10^{-15}$  and the overlap is higher than expected by chance, as calculated by hypergeometric test. Quantitative data are shown in Source Data. Gene sets are provided in Supplementary Data 1.

**Fig. 6**

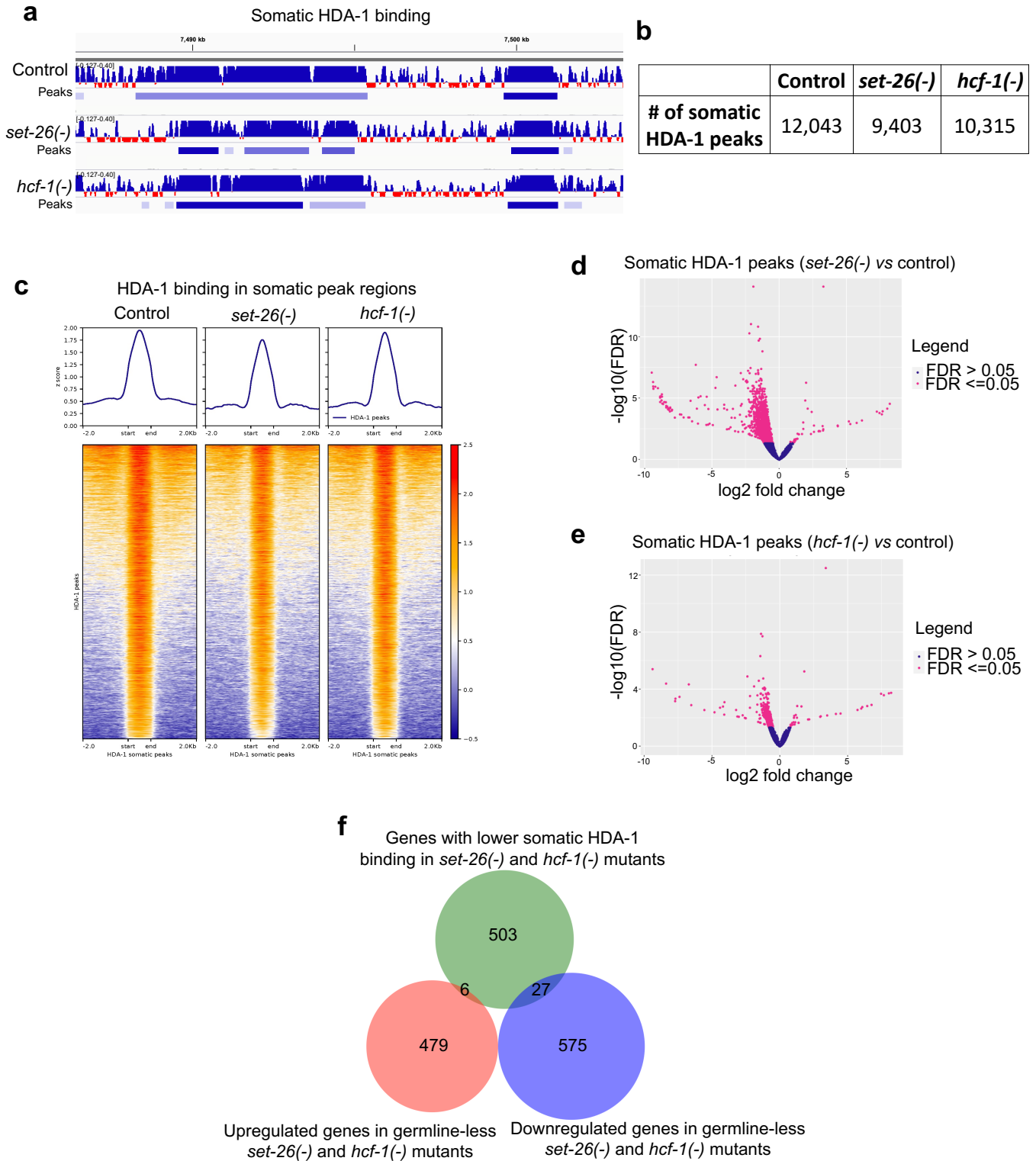


**Fig. 6: SET-26 and HCF-1 are unlikely to be major players in HDA-1's recruitment to**

**chromatin in somatic cells.** **a** Screenshot from IGV shows normalized somatic HDA-1 binding and peak calls in a portion of Chromosome I (captured by CUT&RUN of *hda-1::gfp::ha* worms) in controls, *set-26(-)*, or *hcf-1(-)* mutants grown on *glp-1* RNAi. **b** Number of HDA-1 peaks called in combined replicates of controls, *set-26(-)*, or *hcf-1(-)* mutants grown on *glp-1* RNAi. **c** Metaplot (top) and heatmap (bottom) of z-scores representing normalized HDA-1 signal in somatic HDA-1 binding sites and surrounding 2kb up- and downstream in either controls, *set-26(-)*, or *hcf-1(-)* mutants grown on *glp-1* RNAi. **d-e** Volcano plot of HDA-1 binding regions determined by DiffBind to be significantly different (pink, FDR  $\leq 0.05$ ) or unchanged (blue, FDR  $>0.05$ ) in **(d)** *set-26(-)* or **(e)** *hcf-1(-)* mutants compared to controls grown on *glp-1* RNAi. DiffBind FDR values are calculated using DESeq2. **f** Venn diagram showing the genes with lower somatic HDA-1 binding in *set-26(-)* and *hcf-1(-)* mutants (identified in **d-e**) and the 6 and 27 genes that are commonly up- or downregulated, respectively, in *set-26(-)* and *hcf-1(-)* mutants as determined in Fig. 2a and b. Gene sets and differential peaks are provided in Supplementary Data 2 and 3.

**Fig. 7**

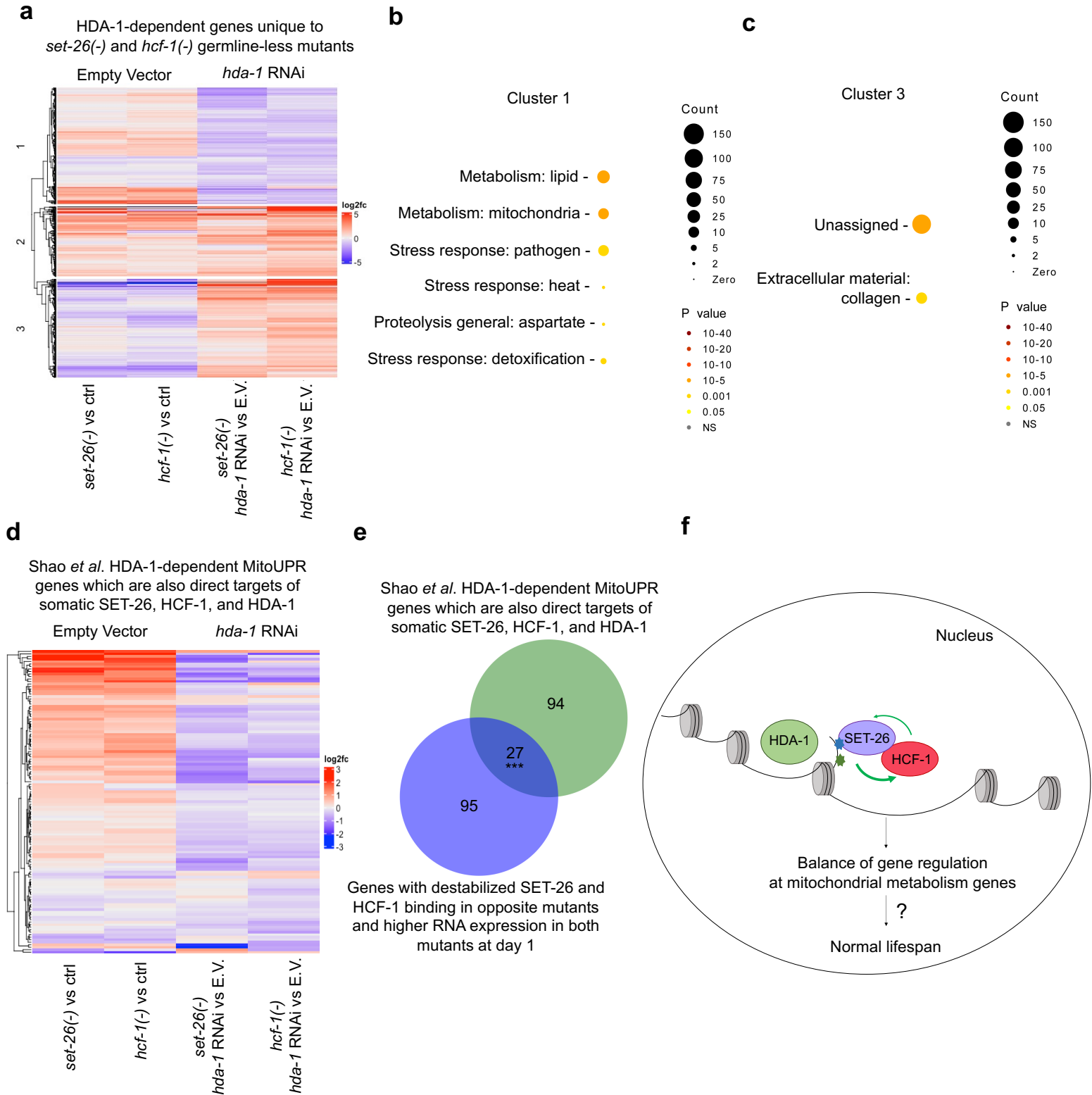


**Fig. 7: SET-26 and HCF-1 control expression of a subset of genes which are co-regulated**

**by HDA-1 in an antagonistic manner. a** Heatmap showing hierarchical clustering of HDA-1-

dependent genes identified as differentially expressed with *hda-1* RNAi specifically in either day

12 adult *glp-1(-);set-26(-)* or *glp-1(-);hcf-1(-)* worms but not *glp-1(-)* single mutants. Log2 fold

change of RNA expression for these genes in day 12 samples are indicated according to the

color scale. Columns 1-2 show expression changes in *glp-1(-);set-26(-)* vs *glp-1(-)* and *glp-1(-)*

*;hcf-1(-)* vs *glp-1(-)*, and columns 3-4 show the expression changes in *glp-1(-);set-26(-)* and *glp-*

*1(-);hcf-1(-)* on *hda-1* RNAi vs E.V. The heatmap is split into 3 hierarchical clusters representing

groups of genes with different behaviors. **b-c** Wormcat GO enrichment analysis of genes

belonging to cluster 1 or cluster 3 as shown in **(a)**. Wormcat *p* values are determined by Fisher

test with FDR correction. **d** Heatmap showing hierarchical clustering of direct somatic binding

targets of SET-26, HCF-1, and HDA-1 that are also genes identified by Shao et al.<sup>13</sup> as “HDA-1-

dependent mitoUPR genes”. Log2 fold change of these genes in our day 12 data set are shown

according to the color scale. As above, columns 1-2 show expression changes in germline-less

*set-26(-)* and *hcf-1(-)* mutants vs controls, and columns 3-4 show the expression change in

germline-less *set-26(-)* and *hcf-1(-)* mutants on *hda-1* RNAi vs E.V. **e** Venn diagram showing

overlap of the common CUT&RUN targets of SET-26, HCF-1, and HDA-1 that are also “HDA-1-

dependent mitoUPR genes” as indicated in **(d)** with the 122 genes on which somatic SET-26

and HCF-1 binding stabilize each other and show higher RNA expression in both mutants as

identified in Fig. 4h. **f** Graphic representing the proposed model, in which SET-26 recruits HCF-

1 to chromatin, where HCF-1 stabilizes SET-26 and the pair work together to regulate the

expression of genes. The model proposes that HDA-1 co-regulates a subset of genes with SET-

26 and HCF-1, often mitochondrial metabolism genes, but in the opposite direction. Together,

the factors contribute to the normal balance of gene regulation and longevity. In **(e)**, \*\*\* indicates

$p < 1 \times 10^{-15}$  and the overlap is higher than expected by chance, as calculated by Fisher’s Test.

Gene sets are provided in Supplementary Data 2.